Multi-Disciplinary Design of an LH2 Powered Regional Jet

Maxwell Stauffer[1], Michael Backlund[1], Zachary Gonzales[1], Julia Koharko[1], Jemima Hadimani[1], Istvan Trakal[1], Calef Putter[1], Veronica Duran Madrigal[1]
and
Timothy T. Takahashi[2]
Arizona State University, Tempe, Arizona, 85281

This paper discusses the design of a regional jet that operates with zero carbon tail-pipe emissions. The zero emissions jet adheres to requirements outlined by both typical airline customers and the Code of Federal Regulations. The team used a MBSE Multi-Disciplinary-Optimization process using *ModelCenter* to integrate and connect design tools together and to facilitate trade studies. The final design, named SkyWhale, resulted in an 88-passenger jet with a high wing, two underwing engines, T-tail configuration and LH2 tanks mounted above the interior. It has an MTOW of 93,663-lbm with a maximum payload of 22,000-lbm, a maximum flight range of 2,100-nM, and a cruise Mach number of 0.76.

I. Introduction

Aviation is responsible for about 3% of global carbon dioxide emissions [1]. As such, there is widespread desire to regulate aircraft tailpipe carbon dioxide emissions. One of the most feasible environmentally-friendly alternative aircraft fuels is liquid hydrogen (LH2). LH2 is an energy carrier, more comparable to a battery rather than an energy source like crude oil. Pure hydrogen can be produced with electrolysis, where water is divided into hydrogen and oxygen by means of electricity. The hydrogen produced from this process offers exceptionally low emissions compared to kerosene, making it a prime candidate for greener aviation.

To configure the aircraft, this team developed tools to address fuselage sizing, stability and control, wing structure, and more. The design initially focused on the sizing of the fuselage since the hydrogen fuel tank and passenger requirements were largely known. From there, weight estimation, takeoff and landing performance, mission performance, and wing structure were able to be developed. Based on these design parameters, the team conducted trade studies on stability, control and drag ensure desirable performance while minimizing weight. If the aircraft's performance was lacking, we would revisit one of the earlier tools until the performance was satisfactory. We often conducted trade studies due to the inherent design interdependency examining how parameter variation affected holistic aircraft performance. For example, although fuselage sizing was approached first, this acted more as a rough starting point and the sizing of the fuselage was revisited multiple times as other parts of the aircraft were developed. The entire design process consisted of refining a design aspect, testing its performance, and relaying those results to the other disciplines. This was repeated with the help of our developed automated tools until the aircraft performance was sufficient and requirements were satisfied.

II. Mission Requirements and Market Study

The team designed a regional jet that operates with zero carbon tail-pipe emissions. This jet will be fueled by LH2 and will aim to replace current operating regional jets that are fueled by kerosene. Although LH2 is a "greener" alternative to current jet fuel, there are several design challenges that come along with it. First, LH2 requires deeply

[1] Undergraduate Student, Aerospace Engineering, School for Engineering of Matter, Transport, and Energy, PO Box 8576106, Student Member AIAA
[2] Professor of Practice, Aerospace Engineering, Arizona State University, P.O. Box 876106, Tempe, AZ. Associate Fellow AIAA

cryogenic conditions to be available in the liquid state. Although LH2 is more energy dense than kerosene, its physical density is much less meaning the storage of LH2 requires about four times greater volume than kerosene to achieve a similar flight range. Along with these challenges, our aircraft must also adhere to all customer requirements in addition to government regulations in the US and Europe. The launch customer for this study were the dominant SkyTeam airline alliance members in the US and Europe (Delta Airlines and KLM/AirFrance). Regional jets flown by these airlines need to seat 70-100 passengers to operate over current route structures.

A. Market Competition

Our market lies in the regional jet market, and all our competitors use fossil fuels. The three jets that specifically compete with us are the Bombardier CRJ 900, the Embraer E175, and the BAE 146-200. Each of these jets sit within the 70-100 seat market but use Jet Aviation fuel in comparison to our plane which uses LH2. Of the three competitors, the E175 has the most range at 2,200-nM. The CRJ 900 and the E175 can climb to max altitudes of approximately 41,000-ft while the BAE 146 can only reach an altitude of 35,000-ft. While the BAE 146 has the greatest payload of the three competitors, it has the slowest maximum cruise Mach ~0.74; we note that the design was specialized for short runway performance. The BAE 146 is also long out of production. The CRJ 900 has not only the lowest MTOW of the three - at 84,500-lbm - but it also has the lowest range of 1,553-nM. The MTOW of the BAE is the largest of the competitors at 93,000-lbm. Also, the take off distance of the E175 and BAE146 are <4,500-ft whereas the CRJ 900 suffers from a very high minimum take off distance of 6,360-ft. The E175 with its many advantages – like great range, short take off distance, high max fuel weight for its class, and great fuel efficiency – makes it stand out as the preferred modern benchmark in this market segment.

B. CFR Requirements

The Code of Federal Regulations [2] presents many regulations that need to be addressed to ensure safe flight. A few of the major requirements pertain to fuel, performance, operational limit loads, stability and control, structural loads and factors of safety, and takeoff/landing. The requirements used for fuel are given in 14 CFR§25.9XX and §121.6XX and performance regulations are given in §25.105. These requirements ensure the plane can perform safely in case of emergencies, such as one engine inoperative. Takeoff and landing regulations are given in § 25.4XX - 25.5XX. Operational limit loads, such as load factors and maneuvering envelopes, as well as speed limitations for maneuvering, flaps, and gear are discussed in §25.1531, §25.150X, and §25.151X. Pertaining to the actual physical design of the aircraft, CFR regulations §25.7XX restrict and mention the safety factors and use of landing gear. For the pitch seating, aisle width, and doors § 25.78X speaks on these regulations. However, there are others to be considered for exits and lavatory size, these are the regulations found in § 25.80X and § 25.8XX for emergency and safety. Finally, while not classified as a CFR regulation, the AC 20-128A specifies the exact distance of engines to the fuselage to ensure the safety of the passengers in case of rotor burst. This also has implications for any high pressure fuel tanks on the aircraft.

C. Flight Routes

As a part of our market study, we researched the typical routes that our target launch customers fly. Our domestic customer, Delta Airlines [3], operates with carrier partners Skywest, Republic Air, and Endeavor Air. Some of the hub airports include LGA (NYC), JFK (NYC), EWR (Newark), MSP (Minneapolis), ORD (Chicago), ATL (Atlanta), and DTW (Detroit). Figure 1 (overleaf) shows the flight route structure for Delta Airlines. Most of the flights remain regional, with most flight distances ranging between 300 and 600-nM. There are a few longer routes that exceed 1000-nM such as the flight between O'Hare and Boise or between Newark and Northwest Arkansas. Some of the shorter routes include flights from LaGuardia to Providence, RI and Charlotte to Charleston and have distances around 100 to 150-nM.

For our European customers, KLM [4] and Air France [5], the hub airports include AMS (Amsterdam), LYS (Lyon), and CDG (Paris). Figure 2 (overleaf) shows the flight route structure for these two airlines. The typical flight distances are fairly shorter than our domestic customer, with most flights ranging between 200 and 400-nM and the longer routes reaching about 600-nM. The shortest routes that our aircraft must operate come from the European customers. The shortest route is the flight distance from Amsterdam to Brussels at just 85-nM.

D. Limiting Range and Runways

We found the equivalent still air distance for all the routes serviced in Figures 1 and 2 [6]. The longest distance that our aircraft needs to fly is from KORD (Chicago O' Hare International Airport, Chicago, IL, USA) to KBOI (Boise Airport, Boise, ID, USA); 1,371-nM. The shortest distance that our aircraft needs to be able to fly is from EHAM (Amsterdam Airport Schiphol, Netherlands) to EBBR (Brussels Airport, Belgium); 85-nM. In general, most of the routes flown by our aircraft have an ESAD in the range of 300 - 600-nM with the average flight distance being about 475-nM. The lowest airport elevation that our aircraft will need to service is -11-ft at EHAM (Amsterdam Airport, NL) and the highest elevation would be about 4,420-ft at KRNO (Reno-Tahoe International Airport, USA). Most of the airports serviced by our aircraft will have an elevation of 0 - 500-ft.

Our market study found which airports constrain takeoff and landing performance. The longest main runway was found to be 14,511-ft long at KJFK (John F. Kennedy International Airport, New York City, USA) while the shortest main runway was found to be 4,948-ft long and is at EGLC (London City Airport, London, UK). In general, most of the main runways at the airports we will be servicing are about 9,000 - 13,000-ft long. Most of the runways that our aircraft will need to be capable of servicing are about 6,000 - 9,000-ft long. These include the main and crosswind runways. Hence, our limiting short runway will be at London City. We need to ensure that all our dry and wet takeoff and landing field lengths, which include the 115% and 167% factored lengths, are able to operate in and out of a ~5,000-ft long runway.

E. Derived Requirements

From analyzing our customers' current operations and market competition, additional requirements were derived for the design of our hydrogen-fuel jet. The market study conducted gave insight to the typical routes that the airlines fly, including flight distances and airport runway lengths. It was determined that the customer flight distances ranged from 85-nM to 1,400-nM, with the average flight distance at about 475-nM. The shortest runway and therefore our constraining runway has a length of 5,000-ft. The market study also covered our jet's competition, which consists of the types of aircraft currently in use by our customers. To remain competitive in the market, we aimed for a passenger seating of 88 and a maximum payload of 22,000-lbm and 1,700-nM ESAD range at maximum payload.

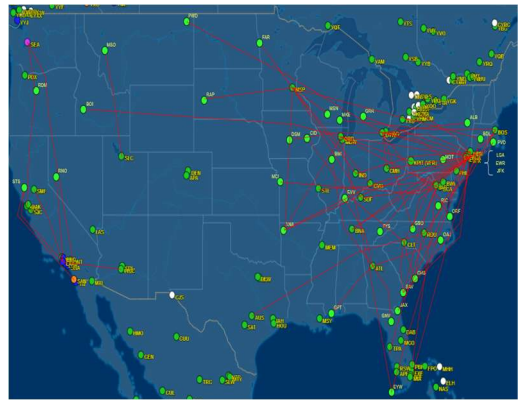

Figure 1. Delta Airlines Flight Route Structure

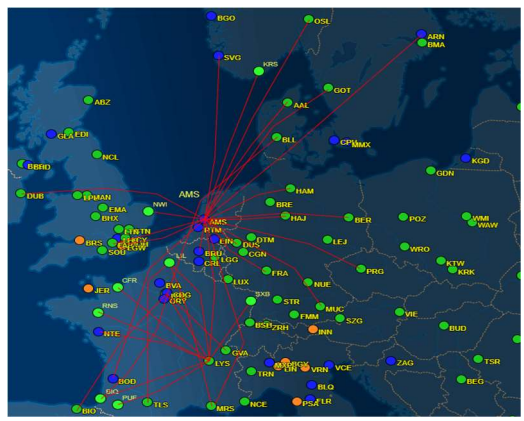

Figure 2. KLM/Air France Flight Route Structure

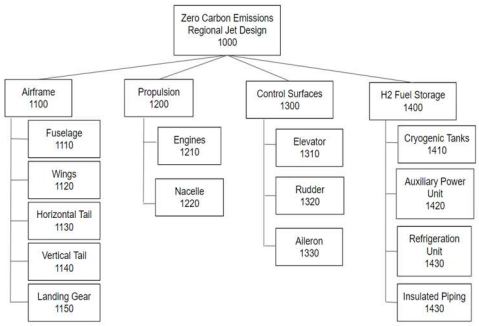

Figure 3. Work Breakdown Structure

III. Design Tools

Figure 3 above shows the WBS for this zero carbon emissions regional jet. The four main branches of the hardware tree include: airframe, propulsion, control surfaces, and LH2 fuel storage. The airframe can be broken down into the fuselage, wings, horizontal and vertical tails, and the landing gear. The propulsion system mainly consists of the engines and nacelles. The control surfaces dictate the static and dynamic stability of our aircraft and consist of the elevator, rudder, and aileron. Finally, the LH2 fuel storage system will consist of the cryogenic tanks, the refrigeration

unit, the auxiliary power unit, and insulated piping. This is one of the most important subsystems of the aircraft as it is mission critical and greatly affects aircraft weight. The most unique part of this aircraft will be the way the fuel is stored and handled as this is the most important novel design feature and part of what makes this aircraft desirable for the customer.

Table 1, below, summarizes the different analysis tools developed for this design project. Each tool is unique and serves a specific purpose in developing the final design. They each have different features that will often depend on one another so connecting the tools is crucial. Also note that each tool was calibrated against known aircraft data to ensure it produces accurate results within acceptable tolerances.

Table 1. Design Tools

1	Torenbeek Weight Code	Estimates the OEW of the aircraft based on various structural parameters. Weight tool has been modified to account for weight of the liquid hydrogen tanks and refrigeration system.
2	EDET Drag	Estimates configuration drag across a large flight envelope based on aircraft geometric inputs.
3, 4, 5	Vorlax Stability and Control	Estimates stability and control derivatives for a given airframe configuration and calculates aircraft cue speeds.
6	Skymaps	Computes vehicle point performance in the Mach-Altitude space using drag data, propulsion data, and aircraft weight.
7	Takeoff/Landing Performance	Predicts the runway limits during takeoff and landing. Considers CLmax and engine scale factor.
8, 12	Wing Structure	Takes the given design values of the aircraft and finds the most efficient thickness and structure of the wing. Describes how loads, shear force, and torque change across the wing's span.
9	Wing Twist	Twists control points on a wing to increase Oswald Efficiency and decrease induced drag.
10	Mission Code	Analyzes missions done by test aircraft and measures performance of test aircraft during mission.
11	Fuselage Thickness	Calculates the minimum skin thickness required for a given combination of material, fuselage diameter, cabin pressure, and operational ceiling.
13	Fuselage Sizing	Calculates required cabin size and associated tank size/weight based on cryogenic storage requirements, material properties, and fuselage/tank integration. Outputs additional data to weight and drag estimators.
15	Wing Aerodynamic Design	Uses VORLAX to compute fine pressures and wing loading based on the thickness, camber, position, and twist of 5 wing profiles (4 wing panels) which informs the aerodynamic design of the aircraft.

A. Weight Estimator

The Torenbeek Weight Estimation tool works by using a variety of inputs relating to the wing and fuselage design as well as information relevant to the propulsion system, cabin pressurization and material properties. It also uses information like the MTOW, MLW and number of passengers as well as reference flight conditions which include the aircraft ceiling. The weight tool uses a set of equations embedded in the spreadsheet to calculate various weight related parameters like the OEW, MZFW, BEW, MEW and flight payloads for a commuter, domestic and international flight. This tool was calibrated using information known about the weights and wing and fuselage design of the Boeing 737 and 747. Subtle changes were made to some of the design inputs which also include the design strength of the material to have the calculated OEW be as close to the published OEW of these aircraft. This tool was then modified to account for the weight of the LH2 tanks as well as the refrigeration system and heavier APU needed. The outputs section of the tool was also modified to get some new valuable weight parameters like the implied maximum fuel weight, standard reserve fuel needed, implied mission fuel weight, minimum MLW and the errors in the MLW and fuel mass on board.

B. Drag Estimator (EDET)

Drag estimation is a critical part in the analysis and design of an aircraft system. This design process utilized the legacy program EDET written by Feagan [8] for Lockheed California. This program takes in parameters that describe the size and shape of key aircraft components and computes a variety of drag data useful for estimating aircraft performance across the entire flight envelope. The program is highly empirical but is known to produce quality results.

This design process used EXCEL/VBA to produce EDET input files and interpret the output files. This allowed for quick integration into linked models. Parametric inputs allow the user to understand drag outputs at all expected Mach-altitude combinations. Inputs include geometry relating to the wing and fuselage in addition to other potential components like tail surfaces, engine nacelles, and engine pylons. The output of EDET includes a zero-lift drag build up table, Reynolds number corrections to the zero-lift drag, a drag polar, buffet CL prediction, induced drag, pressure drag coefficients, and more.

Drag estimation is critical for aircraft performance analysis so the quality of the drag data could not be sacrificed. This tool was calibrated to match known drag data from real world aircraft like the Boeing 737-300 and Boeing 747-100. This involved determining the aircraft geometry and using that to set the primary EDET inputs. Then, the results of the basic run were used to compare to the available data where some parameters were altered to better fit the data. See an example of this in Figure 4 where we tuned the parameters of "Crud Drag" and "AITEK" to best meet the provided data. The calibration is not perfect but tuning this to be as accurate as possible is critical to increase overall model accuracy. This calibration gave confidence to the team that this tool is useful for accurately predicting drag and it can be used for this design project.

C. VORLAX Stability and Control

Making use of VORLAX, which uses a generalized vortex lattice method to accurately predict aerodynamic performance for subsonic and supersonic flow, stability and control derivatives can be found for any given aircraft configuration at various Mach numbers and angles of attack. As such, a tool was designed which allows for a given aircraft configuration to be input or altered, which could then be run through VORLAX, resulting in the stability and control derivatives necessary to determine a given aircraft's longitudinal and latitudinal stability performance. Additionally, using specific values from the resulting data set, the minimum control speeds for takeoff and cruise mode frequencies can also be found. Figure 5 displays the flat plate model of Skywhale used in VORLAX.

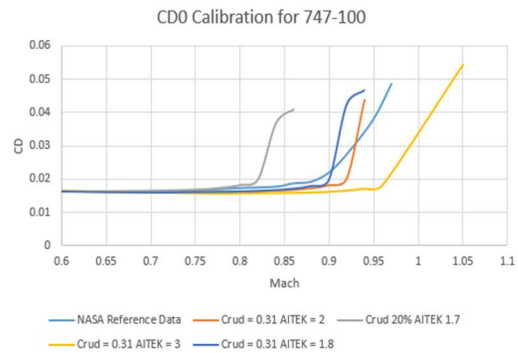

Figure 4. Calibrating EDET Tool Using Boeing 747-100 Data

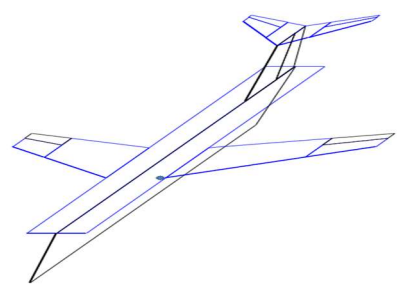

Figure 5. Simple VORLAX flat-panel mockup of final design

D. Five Column Propulsion Performance Data

In order to fully analyze an aircraft design, we need to trade both the size and thermodynamic propulsion cycle of the engine. Here, NPSS [30] was used to develop scalable 5-column datasets for eight engines. NPSS predicted thrust and TSFC as a function of speed, altitude and power-level angle for an LH2 fueled engine with BPR=10; a design point OPR of 45:1, FRP of 1.6:1 and maximum continuous thrust TIT rating at 2,700°R. The performance data was computed assuming a reference inlet recovery efficiency of 99.5%, a design point fan efficiency of 85%, a design point low-pressure compressor spool efficiency of 85%, and a design point high-pressure compressor spool efficiency of 85%. The design point burner efficiency was set to 87% and the high-pressure exhaust-turbine spool efficiency was set to 87%.

Figure 6. Example Point Performance "Skymap" Plot

E. Point Performance Skymaps

The Skymaps tool is a point performance tool that integrates drag information from EDET, propulsion information from the 5-column data released by the engine manufacturer, and a flight weight to predict the aircraft performance at specific points in the Mach-Altitude space. In the case of this project, the propulsion information was provided for a LH2 engine that has a bypass ratio (BPR) of 10:1. The Skymaps tool is able to predict the coefficient, drag coefficient, lift-to-drag ratio (L/D),

Mach-lift-to-drag ratio (M*L/D), percent induced drag, cruise fuel flow, maximum fuel flow, specific range, maximum and minimum thrust, specific excess thrust, rate of climb, and maximum aerodynamic load factor. All of this is very useful to understand the available performance of the aircraft in terms of Mach number and altitude. This tool is most useful to compare changes in different parameters to understand how changes in propulsion, drag, and weight affect point performance. See Figure 6 (previous) for examples from the Skymaps tool.

F. Takeoff and Landing Performance

The takeoff and landing performance tool utilizes Excel Visual Basic to predict the necessary takeoff and landing requirements for an aircraft. It requires inputs such as MTOW, OEW, wing area, and aspect ratio and uses the aerodynamic file from the Drag Estimator tool and the engine propulsion file. From these inputs, the tool is able to predict various takeoff performance requirements, such as minimum dry and wet runway lengths, climb gradient for one engine inoperative, rate of climb, and V2. Equations (1) through (4) briefly show how the takeoff field lengths were calculated.

$$CFL_{dry} = max(750 + 30 * TOP25,3300) \tag{1}$$

$$CFL_{wet} = max(500 + 35 * TOP25, CFL_{min}) \tag{2}$$

$$TOP25 = \frac{W/Sref}{CLmax(\frac{Thrustmax}{W})} \tag{3}$$

$$CFL_{min} = 7700 - 125 * VMCA + 0.928 * VMCA^2 \tag{4}$$

For landing performance, the tool predicts the minimum dry and wet runway lengths needed, including the 115% and 167% factored length, and *Vref*. Equations (5) and (6) briefly show how the landing field lengths were calculated.

$$LDR = 1000 + 0.11 * V_{ref}^2 \tag{5}$$

$$V_{ref} = max(1.23 * V_s, VMCL) \tag{6}$$

This tool shows how these output values vary with different aircraft weights, takeoff and landing lift coefficients, and engine scale factors. It is highly useful in determining what lift coefficients and engine scale factors are necessary for successful operation.

G. Wing Thickness

The wing thickness tool calculates the allowable wing thickness along the span using the simplified 2D Korn equation (7) which has been corrected to account for a swept wing [13]. This tool is intended to take in basic planform geometry and flight conditions to compute an ideal spanwise load, a corresponding spanwise distribution, and then a spanwise thickness distribution using a chord distribution, an ideal C_L distribution, and the flight conditions. Some of the other outputs obtained also include the aspect ratio, calculated for a basic trapezoidal planform, as well as the Mach number normal to the leading edge of the wing.

$$t/c = K * cos(Wing_{SWP}) - 0.1c_L - (DesignMach - 0.05) * cos(Wing_{swp})^2 \tag{7}$$

H. Mission Performance (Mission Code)

The Mission Performance tool uses an aero file, a propulsion file, and a mission code file to analyze the performance of a plane's configuration. The program utilizes ModelCenter and the Execl/VB mission code which uses aero, propulsion and mission command text files. The user starts by defining the Mission File Writer variables, and then defining the aero file, the propulsion file, and the mission file fields within the Mission Code component. Then the user can run any trade studies necessary to evaluate their current configuration; see Figure 7.

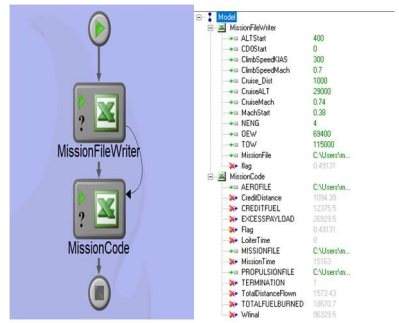

Figure 7. Mission Performance in ModelCenter

I. Wing Structure

The wing structure tool pairs with the wing thickness chooser to provide values concerning the wing torque box and the applied loads experienced by the wing. It takes inputs from the thickness chooser such as the thickness to chord ratio from Korn's equation, the running load across the span, and the chord length across the span. It also considers the material strength, sweep angle, and maximum load factor. The tool can compute important values across the span including the max thickness of the wing, the shear force and bending moment, the minimum cross-sectional area, and the skin thickness. The dimensions of the wing torque box are then able to be calculated using these outputs.

NPASS	88		Fuselage Width	172	in
C1PASS	27		Fusleage Height	188	in
C2PASS	61		Min. Radius	86	in
PercentClass1	0.3				
C1Pitch	36	in	C1 Rows	7	
C1Width	22	in	C2 Rows	13	
C2Pitch	31	in			
C2Width	20	in	Door Fore Width	48	in
			Door Aft Width	48	in
C1 Pax/Row	4				
C2 Pax/ Row	5		Ref. P (psi)	7	* Local ATM
Aisle Width	24	in	Min. Steel thick (in)	0.03	
Aisle Count	1		Min. AL thick (in)	0.03	
Lavatories	2				
Lavatory Length	48	in	Fuselage Length	1115	in
Galley Length	48	in		93	ft

Figure 8. Fuselage Cabin Sizing Inputs

J. Fuselage Thickness

The Fuselage Thickness tool is an EXCEL spreadsheet which takes inputs for fuselage diameter, material properties, cruise altitude, cabin pressure altitude. Using these values in conjunction with the hoop stress equation, the minimum thickness of the fuselage can be calculated, limited by CFR requirements and a set minimum gauge thickness. This contributes to an understanding of the structural requirements of the fuselage and if it is reasonable to design.

Total Fuel Mass	8608.8044	lbm		Equivalent Energy Kerosense We		24425.76	lbm
Total Fuel Volume	14560.811	gal		Combined Tank Weight		7269.573	lbm
3	% of req.	121%		* Not including refrigeration system weight or other			
1	2	3	4	5	6	7	8
387	387	387	219	219	219		
56	56	56	56	56	56		
1.5	1.5	1.5	1.5	1.5	1.5		
53	53	53	53	53	53		
808198.53	808198.53	808198.53	437559.72	437559.72	437559.72		
3498.695	3498.695	3498.695	1894.1979	1894.1979	1894.1979		
3148.8255	3148.8255	3148.8255	1704.7781	1704.7781	1704.7781		
1861.6836	1861.6836	1861.6836	1007.9179	1007.9179	1007.9179		
99009.649	99009.649	99009.649	55863.015	55863.015	55863.015		
-410	-410	-410	-410	-410	-410		
140	140	140	140	140	140		
20	20	20	20	20	20		
120	120	120	120	120	120		
13	13	13	13	13	13		
SS AM-350	SS AM-350	SS AM-350	SS AM-350	SS AM-350	SS AM-350		
5	5	5	5	5	5		
366000	366000	366000	366000	366000	366000		
176400	176400	176400	176400	176400	176400		
117600	117600	117600	117600	117600	117600		
14	14	14	14	14	14		
0.031	0.031	0.031	0.031	0.031	0.031		
559.22511	559.22511	559.22511	314.54437	314.54437	314.54437		
2024-T3 Aluminum	2024-T3 Aluminum	2024-T3 Aluminum	2024-T3 Aluminum	2024-T3 Aluminum	2024-T3 Aluminum		
1	1	1	1	1	1		
64000	64000	64000	64000	64000	64000		
47000	47000	47000	47000	47000	47000		
31333.333	31333.333	31333.333	31333.333	31333.333	31333.333		
0.03	0.03	0.03	0.03	0.03	0.03		

Figure 9. Tank Sizing Inputs and Outputs

K. Fuselage and Tank Layout

The fuselage layout tool accounts for the fuselage size requirements from the cabin as well as integration of the cryogenic fuel tanks. It was known early on that the fuel storage will likely have to be in the fuselage so a unique tool is best for this design task.

This tool takes inputs for the passenger compartment (passenger number, seat size, seats per row, etc.), required dimensional lengths (amenities, structure, cockpit, doors, added "crud" length), and tank parameters (external diameter, storage temperature, insulation pressure, tank materials, minimum gage, etc.) to compute the corresponding fuselage size and tank size to include tank weights and fuel capacity. The outputs from this program flow primarily to drag and weight estimation accounting for exterior dimensions and weights that are used in the tools. The concept is to allow easy parameterization of inputs so that integrated trades are possible.

The first section of this tool includes requirements for the pressurized cabin which sets the primary size of the fuselage. An example of this is in Figure 8 for reference where the user can input dimensions and other numbers relating to the cabin size. This is where users can ensure regulatory compliance with seating arrangements and passenger accommodations.

The next section of this tool focuses on the tank sizing which is driven by the fuselage size and engine placement. Fuel tank placement was set early on to be above the pressurized cabin. This is because wing-mounted fuel tanks are not realistic, nor will they carry all of the required fuel given the wing size and the fuel storage requirements. Tanks

mounted above the fuselage are preferable as a hard landing situation with broken gear and low-mounted tanks would result in the aircraft landing on the tanks and more likely igniting the fuel. Engine placement drives the fuel tank size because the tanks must not be within the rotor burst zone as dictated by AC 20-128A. Thus, the allowable tank length is set by the available fuselage length and the position of the motors relative to the fuselage allowing for 15° of clearance from all rotating turbomachinery.

The user can then set the volume and weight of the fuselage tank through another set of inputs focusing more on the tanks directly. In this section, the user can change the external diameter of the tanks, the material choice, and a couple other parameters to set the internal size and weight of the tanks. Reference Figure 9 (previous) for sample inputs considering a set of 3 forward tanks and 3 aft tanks set by fuselage and engine size/placement. The storage method for the fuel assumes two concentric pressure vessels where the first tank contains the fuel at cryogenic conditions (in liquid phase as determined by [9]) and the second tank contains the first tank as well as an insulating noble gas like Xenon at a non-zero pressure to ensure all tanks have internal pressure (external pressure tank design is not easily parameterized, nor it is lightweight). This tool accounts for 10% overpressure of the tanks to ensure the fuel is in the liquid phase and 10% ullage volume from [9]. The tank thickness is calculated using the same methods from the Fuselage Thickness tool (hoop stress with safety factors) but considers the change in material properties at cryogenic conditions from MIL-HDBK 5J [10]. This completes the parametric sizing tool for the combined cabin-tank fuselage used in later trade studies and design.

L. WINGLETS (Aerodynamic Wing Design)

WING Lean Evaluation and Technical Synthesis (WINGLETS) is an EXCEL/VBA tool that utilizes VORLAX [11] to complete the fine aerodynamic design of aircraft wings. This tool can accommodate 5 wing control points along the span while varying the sweep, chord, dihedral, thickness form, camber form, and twist. All of this contributes to the freedom to design a wing for nearly any situation. The tool contains a small library of common NACA thickness and camber forms primarily from NACA 824 [12] to open the design space for a given wing. The tool interprets outputs from VORLAX to understand aerodynamic performance of the wing such as the design lift coefficient, spanwise loading, and chordwise pressure contours at specific span locations. This tool also pairs with a companion MATLAB script to understand the upper and lower surface pressure contours for a specific flight condition. Reference Figure 10 for example wing inputs for a given set of thickness and camber forms; program outputs are visible in the later wing design section.

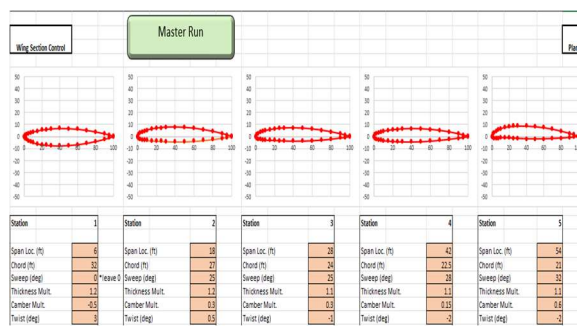

Figure 10. Sample Inputs for WINGLETS Program

M. Connecting Tools

The system functional decomposition is found in Figure 11. Figure 12 (overleaf) shows how *ModelCenter* was used to link multiple excel sheets and scripts to run trade studies. Trade studies allow us to study the effects of certain variables on the performance of a vehicle configuration. ModelCenter connects the sheets as shown above and can automate the completion of trade studies under certain commands.

The configuration manager tool was developed in Excel and consists of our basic aircraft sizing inputs for the wings, fuselage, propulsion system and the horizontal and vertical tails. This tool also contains information on our reference flight conditions. The information from the

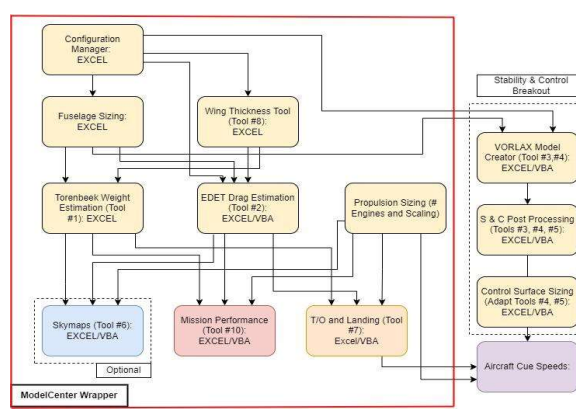

Figure 11. System Functional Decomposition

configuration manager is then used in the fuselage sizing, wing thickness and EDET drag estimation tools which were developed in Excel and VBA.

The fuselage sizing tool calculated the required cabin size and tank sizing parameters based on the storage requirements of the cryogenic fuel system as well as the material properties of the fuselage and cryogenic tanks.

The wing thickness tool finds the optimal thickness and structure of the wing which will ensure that shocks aren't formed on the wing surface. This tool also shows how various loads, shear force and torque change across the span of the wing.

The EDET drag estimation tool estimates the drag across a large flight envelope based on the aircraft's sizing inputs.

Inputs and results from the fuselage sizing tool are then used in the Torenbeek Weight Estimation and EDET drag estimation tools. The Torenbeek Weight Estimation tool estimates the OEW along with other fuel and MLW related weights based on various structural parameters. The original weight tool has been modified to account for the weight of the cryogenic fuel storage system which includes the weight of the LH2 fuel tanks and the refrigeration system. Inputs and results from the wing thickness tool were used in the EDET drag estimation and Torenbeek weight tool to further predict all the required weights and drag and lift related parameters. A simple propulsion sizing tool helped determine the optimal number of engines and engine scale factor to ensure the best mission point performance as well as landing and takeoff performance.

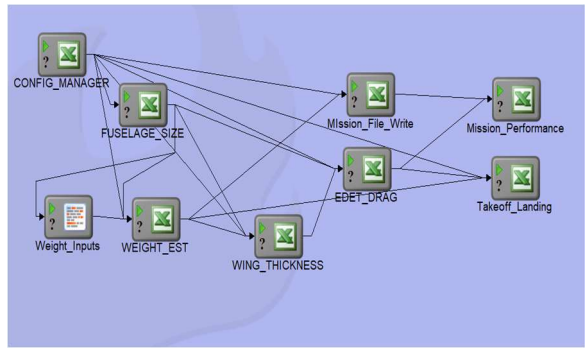

Figure 12. Combined ModelCenter Model

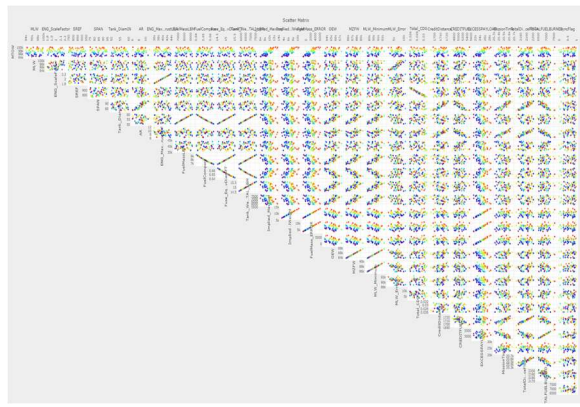

Figure 13. Overall Interaction of Sizing Parameters

Inputs and results from the Torenbeek Weight estimation, EDET drag estimation and propulsion sizing tools are then used in the Skymaps, mission performance, and takeoff & landing tools. The Skymap tool computes the point performance of the aircraft in the Mach-altitude space using drag, propulsion and weight data. The mission performance tool analyzes the performance of a test aircraft for a simulated mission. The takeoff and landing tool predicts the runway performance using various maximum lift coefficients and engine scale factors.

We can also use a VORLAX model to estimate stability and control. The results from the VORLAX model supported sizing the control surfaces of the aircraft. All the results obtained from the stability and control breakout and the propulsion sizing tool are used to predict the aircraft cue speeds which will influence the various takeoff speeds used to predict the takeoff and landing performance of the aircraft.

IV. Trade Studies

A. Aircraft Sizing

This aircraft has novel features so it is important to consider the sizing carefully as it could be different from a typical kerosene-powered commercial aircraft. The sizing study for this aircraft uses the combined ModelCenter data model to vary chosen parameters and examine the corresponding outputs. This trade was not necessarily wide in scope but only focused on ranges of values that were reasonable given the target number of passengers and range requirements.

The baseline for this trade study is an aircraft suited to accommodate 88 passengers on regional routes. This baseline has a sufficiently large tail for stability and a configuration resembling that of the final design. The fine details of the design would not have significant implications on the target outputs for the aircraft and it is expected that any reasonable configuration for a similar commercial aircraft would have similar results. The full results of this trade are in Figure 13 (previous) which is a scatter matrix of all inputs and outputs which illustrates noticeable trends. From this, we selected more specific interactions to examine and shape the design.

Aircraft field performance is a critical consideration as there are several important runways that are relatively short from the market study section. Thus, considering the effect of two major sizing parameters, Maximum Takeoff Weight (MTOW), and Wing Reference Area (Sref), will provide understanding on what is actually possible to fly on target runways; see Figure 14. We see here how more weight and less wing area relate to worse field performance; our design must work to reduce weight and increase wing area to a reasonable value.

The interaction in Figure 15 demonstrates that MTOW clearly drives implied fuel mass which is from a weight perspective but this is not necessarily the amount of fuel allowed by the tanks. Additionally, the allowable tank volume (dictated by tank diameter in this case) is a contributor to Operational Empty Weight (OEW) and thus MTOW. This means that the design must strike a balance between the allowable fuel mass from a weight perspective and the corresponding fuel volume from the tank size. This interaction is factored into the combined model to ensure that the intended aircraft weight can accommodate the required mission fuel and necessary reserve fuel.

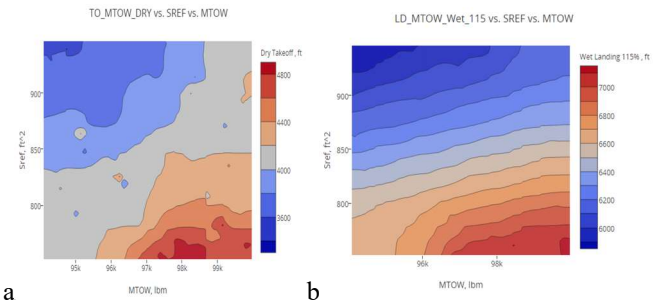

Figure 14. Field Performance Trades: a) Takeoff, b) Landing

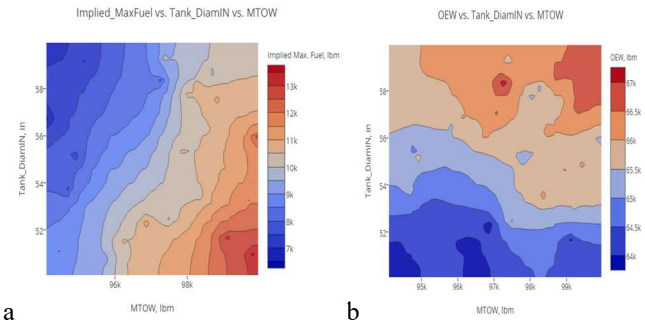

Figure 15. MTOW and Fuel Tank Diameter Impacts on a) Fuel Capacity b) OEW

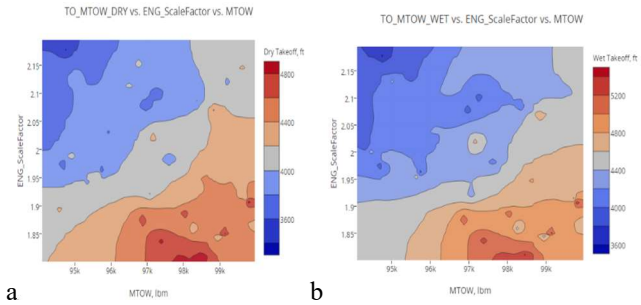

Figure 16. TOW and Engine Scale Factor Influencing a) Takeoff Length and b) Landing Length

Another important interaction is in Figure 16 between the aircraft MTOW and the engine scale factor. The thrust is an obvious factor in takeoff performance from a conceptual level but results from the takeoff and landing tool indicate that these engines are not as significant. This is an artifact of the method used to predict takeoff and landing lengths from Takahashi [13] where the aircraft is not struggling to meet the takeoff requirements (always less than ~5000-ft). This effectively means that the engine scale factor is not a significant driver to takeoff length and must be sized by cruise conditions from detailed mission simulation.

B. Fuselage and Cabin Sizing

Fuselage sizing trades used the fuselage sizing tool mentioned above to examine how this design can configure the fuselage to best meet all mission and operational requirements. Since the fuselage is the core of this aircraft this study

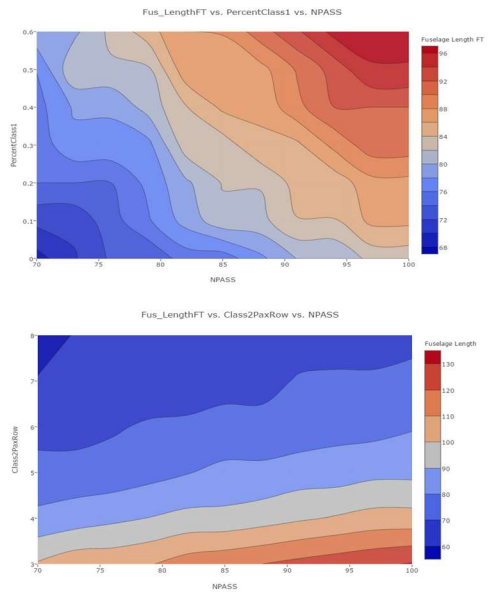

Figure 17. Interaction of Passenger Count and Seat Configuration on Fuselage Length

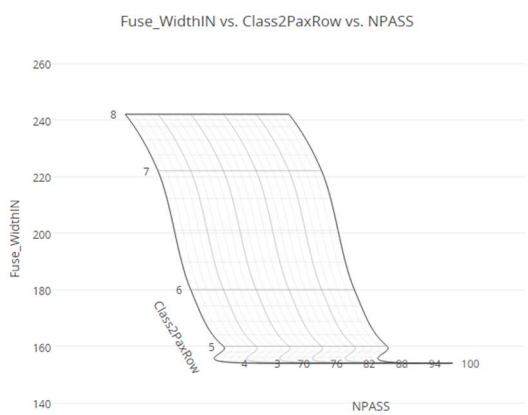

Figure 18. Trend of Overall Fuselage Width vs. Passengers per Row

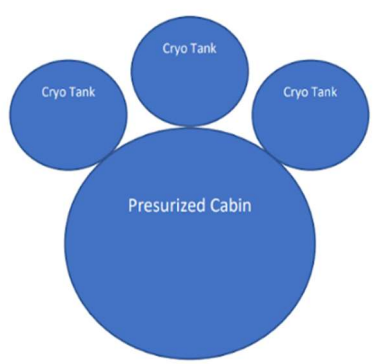

Figure 19. Cryogenic Tank Configuration

is critical and allows greater insight on the interaction between competing factors in fuselage integration. These competing factors are passenger and door arrangement, amenity integration, cryogenic tank integration, and rotor burst zone integration. The focus on fuselage sizing is to set the cabin to a proper size given the mission and regulatory requirements which will then affect the fuel tank sizing.

The interaction in Figure 17 demonstrates the relationship between passenger count and fuselage seating information on the fuselage length. The number of passengers has a clear effect on the fuselage length in addition to the number of first-class seats, and passengers per row in the economy class. This length is a direct contributor to the wetted area whereas the width (dictated in part by passengers per row) contributes to the maximum cross sectional area. Both have important drag considerations. The goal is to reduce drag which translates to a minimization of fuselage wetted area and maximum cross section (form factor). Our design considers this in addition to self-imposed limitations such as having 5 passengers per row to accommodate space for luggage/cargo under the passenger compartment.

The selection of passengers per row sets the cabin width (with additional width for structure and other needs) which may not be the overall fuselage width. Recall that the fuselage will include the presence of tanks arranged above the pressurized cabin which may contribute to the overall width and will contribute to overall fuselage height. Reference Figure 18 for this interaction on fuselage width noting that the presence of the tanks may limit the overall width if the passengers/row is too low.

The requirements of the cabin primarily drive the size of the fuselage which is important to consider in this design. However, the cryogenic fuel tanks are a system-critical addition to a regular fuselage that must play into the corresponding size of the cabin thus the passenger requirements are not to be considered alone in fuselage design.

C. Tank Sizing

In most aircraft, the fuel is stored in the wings; however, because we are using hydrogen as fuel, our aircraft requires tanks of about four times the volume of a typical kerosene tank. Instead of storing the hydrogen fuel in the wings, we designed a tank configuration above the fuselage. This design consists of three smaller round tanks shaped around the fuselage, see Figure 19. When running these trade studies in the Fuselage and Tank tool, it was already determined that the fuel tanks would be on top of the fuselage. The trade focused on how the fuel should be broken up in the number of tanks and their size. This was resolved prior to PDR and concluded that three tanks with

a diameter size of 50-60-in each provided enough fuel for missions while not significantly increasing the total weight of the aircraft, as the tanks would have a cooling system as well.

From these studies we were able to find that larger tanks were more weight efficient, as there is less material used up to create several tanks, see Figure 20. It was also found that the weight of the aircraft was more material dependent than fuel. This is expected as the material properties may vary heavily. Trade results also found that the number of tanks does not have a significant effect on the entire system weight holding the fuel volume constant. Thus, we struck a balance between 4 radial tanks, which are less weight efficient from smaller diameters, and 2 radial tanks, where the fuselage cross section becomes too rectangular.

The ideal material for the tanks was found to use SS AM-350 for the internal shell and 2024-T3 Aluminum for the external shell. See Figure 21 for the trades relating to material type.

D. Engine Placement

Rotor burst safety concerns from the FAA dictate that the cryogenic tanks shall not be in the engine rotor burst zone. Several trades were run to determine how the engine placement affects the length of the forward and aft fuel tanks, as well as the weights of these tanks. The results of this study show that as the engines move up, the lengths of the forward and aft fuel tanks must decrease and increase respectively. This placement affects the center of gravity of the aircraft and thus must be considered in the stability and control analysis. The diagram in Figure 22 depicts this.

E. Wing Thickness and Camber

When designing the wing, its thickness was paramount in keeping the wing performing efficiently at near transonic Mach numbers. The larger the thickness, the earlier the onset of shock waves and, in turn, wave drag. The design of the thickness was done iteratively, as whether the thickness was sufficiently sized was dependent on the magnitudes of the upper surface pressure coefficients being less than that of the critical pressure coefficient.

The results from changing the maximum thickness of the wing show that an increase in the thickness causes an increase in the magnitude of the peak suction; see Figure 23 (overleaf). Keeping this peak suction value under the critical pressure coefficient was necessary along the entirety of the span, and the thickness was tweaked at multiple control points to achieve this.

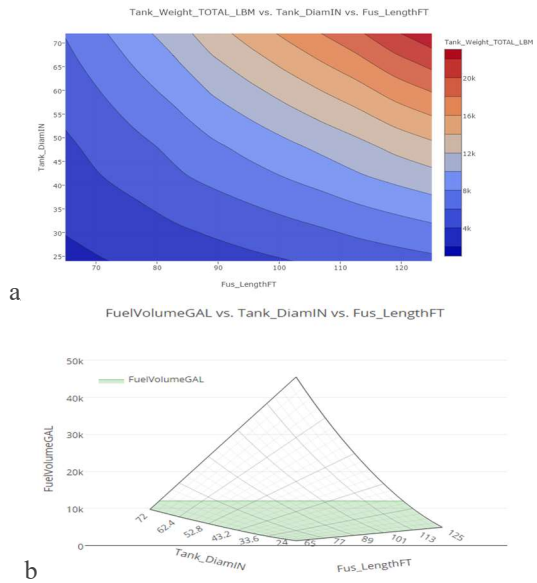

Figure 20. Fuselage Length and Tank Diameter a) Tank Weight, b) Fuel Volume

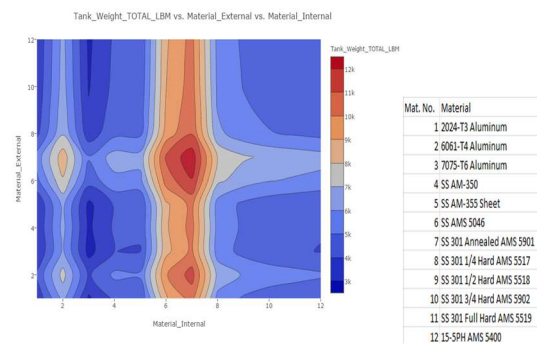

Figure 21. Material Type Tank Weight Trades

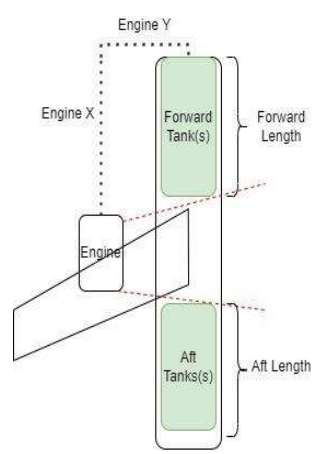

Figure 22. Engine Placement-Tank Diagram

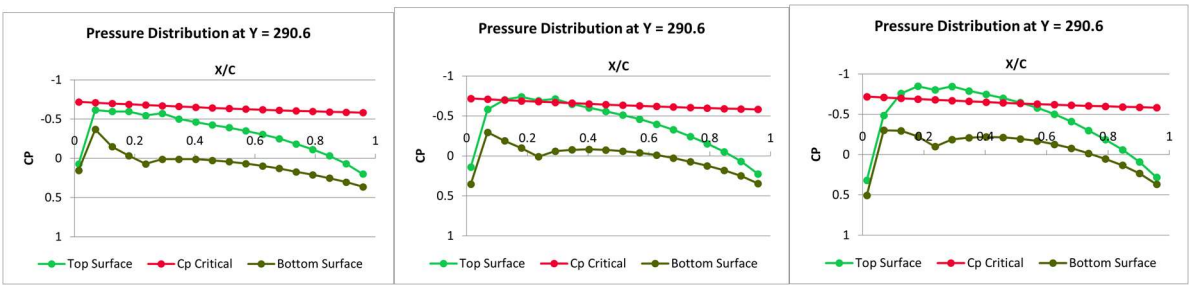

Figure 23. Pressure Distributions for Varying Maximum Thickness from 5% to 15%

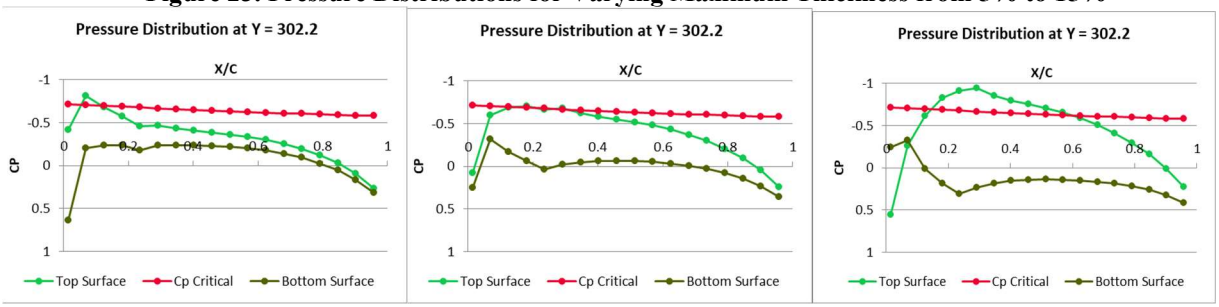

Figure 24. Pressure Distributions for Varying Maximum Camber from 0% to 2.2%

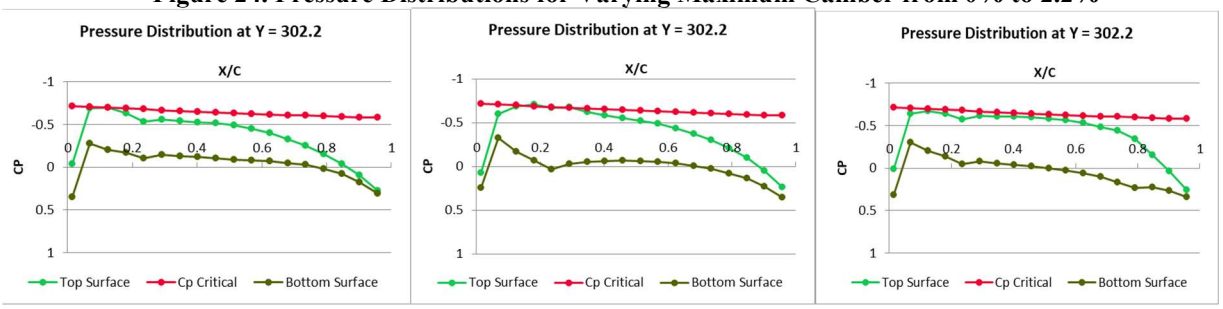

Figure 25. Pressure Distribution for NACA 230, NACA 63, and NACA a = 0.8 Camber Lines

Testing different maximum camber percentages was useful in understanding trends in regard to camber. The NACA 63 airfoil, which has a max camber of 2.2% at 50% chord, was used as a baseline for this trade study. Three camber magnitudes were applied to this airfoil, resulting in 0% camber, 1.1% camber, and 2.2% camber; see Figure 24. Higher camber, although producing more lift, causes pressures that exceed the critical pressure coefficients inducing shock formations. Lower chamber, although comfortably satisfying the critical pressure coefficient requirement, may struggle to produce enough lift to match the idealized elliptical lift distribution. So, the camber must be balanced such that both critical Mach number requirements and lift requirements are met.

The camber line was also adjusted to see its impact on the pressure distribution; see Figure 25. The result of the trade indicates that changing the camber line changes the overall shape of the pressure distribution and the location of the peak suction. It seems pushing the location of the maximum camber further along the chord pushes the location of the peak suction further back as well. Thus, using a camber profile that keeps the peak suction below the maximum critical pressure coefficient is necessary.

F. Drag Source Trade Studies

Multiple trades were run for several different configurations of the aircraft's main body components, including the wing reference area, empennage component dimensions, fuselage dimensions and others. Making use of EDET in conjunction with ModelCenter, the geometries of these various components were varied through a range of plausible values for the potential final design of the aircraft, and the resulting relationships were used to guide the development of the aircraft.

The results from these trades were almost entirely expected, as the drag increased solely with an increase in surface area for most cases; see Figure 26. There are a few stand out cases, these being the effect of increasing wing reference area, fuselage area, and changing the taper ratio and sweep angle of the wing. For increasing the wing reference area, the increase in drag is not linearly related as it is with the other cases. This makes sense given that the drag of an aircraft is dependent on the reference area, such that, while increasing the area increases the drag, it also decreases the drag coefficient for resulting in a nonlinear relationship between the dimensional drag and the reference area.

The fuselage has similar non-linear relationships due to the fineness ratio changing with a change in the diameter or length of the fuselage. From the results, we can see that a 50% increase in fuselage length increases the drag just slightly less than a 30% increase in the diameter of the fuselage, meaning that, in terms of space, it would be better to increase the length of the fuselage than the diameter. Finally, there is some drag dependence on the taper ratio and sweep of the wing, though the effect is minimal in comparison.

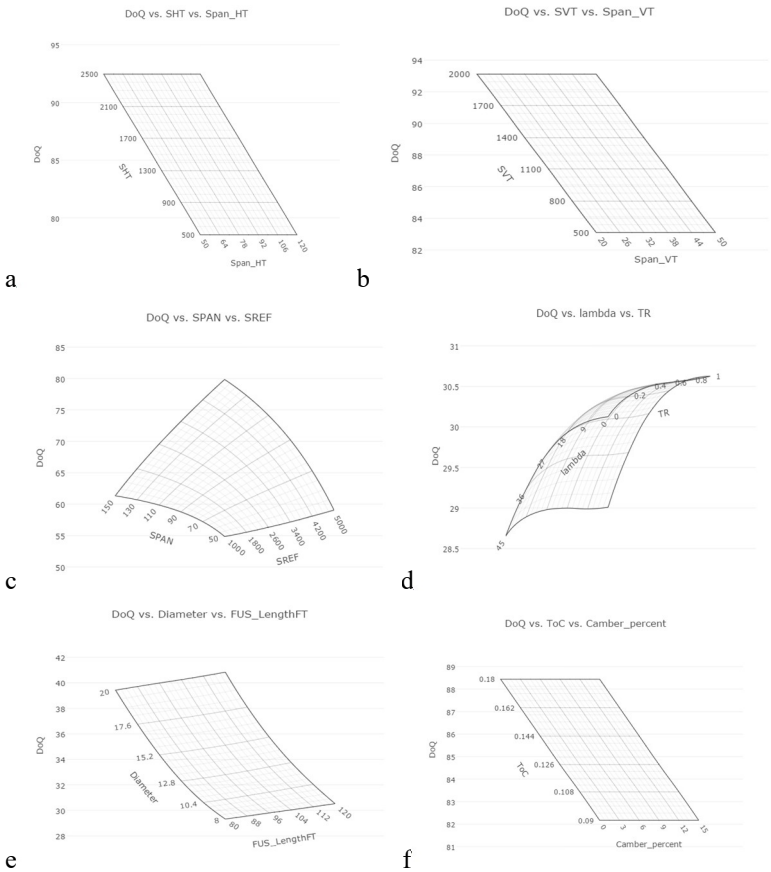

Figure 26. Drag trade Results for Various Components

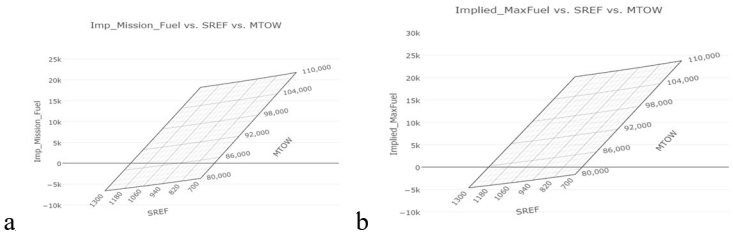

Figure 27. Implied Mission and Maximum Fuel as a Function of Wing Reference Area and MTOW

G. Weight Trade Studies

To estimate the weight of our aircraft, some of the most important parameters that play a significant role in determining important weights that need to be considered when flight planning is the wing reference area, MTOW and MLW of the aircraft. Figures 27a and 27b show the trends in the implied maximum and required mission fuel for an average flight mission of about 475-nM as well as the smallest allowed MLW required for the aircraft to land. From Figure 27a, it is observed that in general, the implied maximum fuel increases as the wing reference area and MTOW of the aircraft is increased. It is also observed that for an MTOW of 82,000-lbm and lower and a wing reference area ranging from 700-ft^2 to 1,200-ft^2, the implied maximum fuel will have a negative value which means that in general, our aircraft will not be able to fly if its MTOW is lower than 82,000-lbm. From Figure 27b, it is observed that increasing the MTOW and wing reference area increases the implied mission fuel required for an average mission distance of 475-nM. It is also observed that the implied mission fuel required for an average flight distance of about 475-nM and an MTOW of generally 87,000-lbm and lower would result in a negative implied mission fuel which means that the aircraft cannot successfully complete the mission.

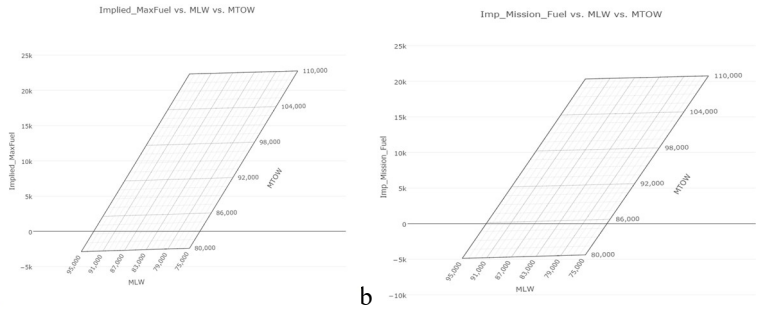

a b

Figure 28. Implied Maximum and Mission Fuel as Function of MLW and MTOW

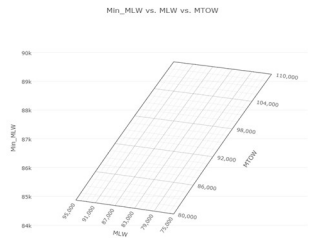

Figure 29. Minimum MLW as a Function of MLW and MTOW

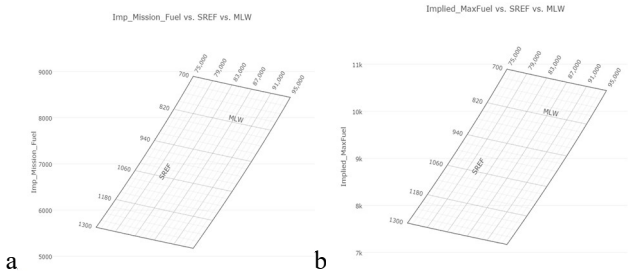

a b

Figure 30. Implied Mission and Maximum Fuel as a Function of Wing Reference Area and MLW

Figure 27 shows that in general, as the wing reference area and MTOW are increased, the required smallest MLW generally increases. A larger MLW and MTOW would mean that a longer runway is required for landing, and this may become problematic at some of the smaller operational airports. The takeoff and landing field performance would decrease as these weights increase, particularly at airports where we are limited by the available runway lengths in the dry and wet conditions.

Figures 28a and 28b below show the trends in the implied maximum and required mission fuel as a function of the MLW and MTOW. These figures show that as the MLW of the aircraft is increased, the implied maximum and required mission fuel mass decreases slightly. An MLW range of 75,000 to 95,000-lbm was used to run these trade studies. It is also observed that increasing the MTOW of the aircraft increases the implied maximum and mission fuel. This means that the MLW of the aircraft doesn't heavily influence the implied maximum and mission fuel, compared to the effect of the MTOW on these fuel weights. These figures also verify the results found in Figures 27a and 27b earlier i.e. for an average flight distance of 475-nM, the implied maximum fuel mass is negative for an MTOW smaller than 82,000-lbm. We also see that the implied mission fuel mass is negative for an MTOW smaller than 86,000-lbm. Figure 29 shows the trend in the smallest allowed MLW as a function of the MLW and MTOW. Figure 29 shows that in general, as the MLW and MTOW are increased, the required smallest MLW generally increases. This would again mean that a longer runway would be required to land and this may become an issue at the airports that limit our takeoff and landing performance.

Figure 30 demonstrates how the implied maximum and required mission fuel loads change as a function of MLW and wing reference area. As MLW increases, the implied maximum and required mission fuel mass decreases. It is also observed that increasing the wing reference area of the aircraft for any given MLW generally decreases the implied maximum and mission fuel weights.

H. Tail Sizing

The driving factor in the design of the empennage structure and sizing was keeping the aircraft within the "A" zone of a Bihrle-Weissman chart, signifying that it is both highly departure and spin resistant, as well as ensuring our crosswind performance remains acceptable. The vertical tail played the largest part in the aircraft's performance with respect to this, as changing the root chord length or the height changed the CnBeta_dynamic and LCDP performance relatively significantly. However, increasing the height of the vertical tail resulted in worse crosswind performance, meaning a balance between the root chord and height had to be struck to meet the performance goals stated earlier.

As such, trades were run with multiple chord and height pairings until a sufficient design was found for the vertical tail.

Figure 31 shows that, when limited by 20% of the stalling speed, there are many different sizes of the vertical tail which could have been chosen. However, to keep both VMCA and VMCG values low, a size which provides just enough crosswind performance would be optimal. This optimal sizing depended heavily on its capability to keep the aircraft departure and spin resistant for any possible flight condition and takeoff weight and as such, various configurations had their performance measured on a Bihrle-Weissman chart. Through repeated runs, the final vertical tail configuration was determined.

In designing the horizontal tail there was much more freedom in determining its configuration. First, determining the configuration of the empennage structure as a whole needed to be carried out. As the fuel tanks were mounted on top of the fuselage and extend far aft of the aircraft, whether there were going to be adverse effects on the flow over the horizontal tail in a normal configuration was uncertain. This uncertainty was what caused a T-tail configuration to be considered, at which point the performance of a control configuration for both empennage types was tested. The results from this test showed that the T-tail configuration was ideal, as it improved crosswind performance with little change to the overall stability of the aircraft. That being the case, combined with the uncertainty of the aerodynamics of a normal configuration, the T-tail configuration was chosen.

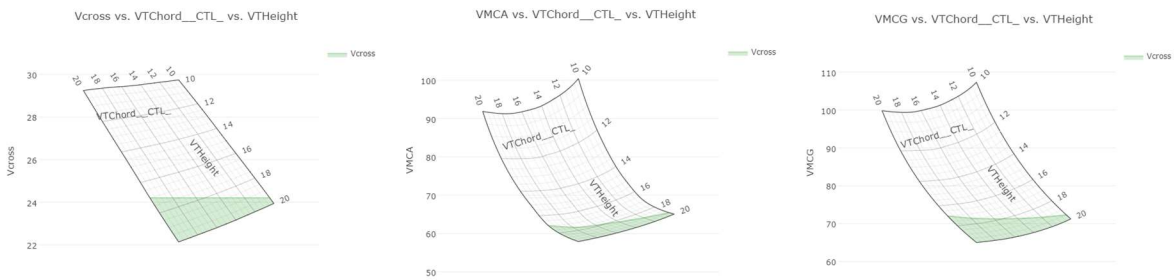

Figure 31. Control Speed Results Due to Varying Vertical Tail Size

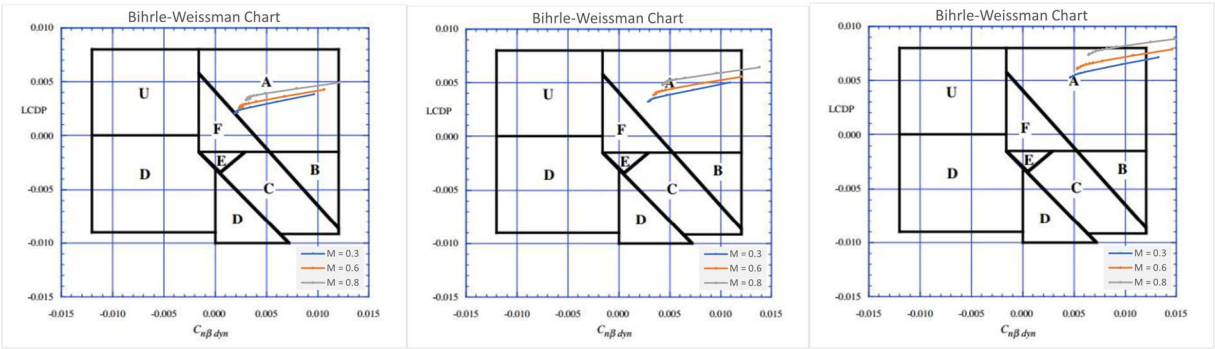

Figure 32. Bihrle-Weissman Chart for a Smaller, Mid-Size, and Larger Vertical Tail Size

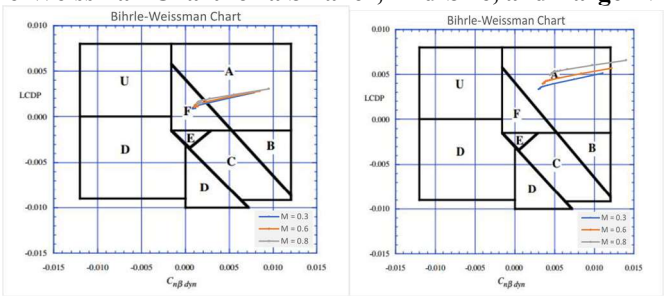

Figure 33. Bihrle-Weissman Chart for Standard Tail and T-Tail Configuration

When sizing the horizontal tail, there was very little response from VMCA and VMCG when changing the span and chord relative to the vertical tail and the crosswind performance was adequate provided the tail was not too large. As such, the driving force for deciding the horizontal tail's size was ensuring that pitch stability was met and, once again, that the aircraft remain departure and spin resistant, as there was some response in the Bihrle-Weissman chart due to the horizontal tail dihedral adding effective height to the vertical tail. To that end, individual cases were run for varying cases to see the effect of changing the span and chord of the tail on the pitch stability and departure and spin performance. This continued until an adequate design was found.

I. Rigid Body Frequencies and Control Speeds

To have adequate control speeds and cruise mode frequencies, the various control surfaces on the aircraft must be properly sized and the sweeps and taper ratios of the wing and tails must be adequately designed. Trades were conducted to vary these control surface sizes, sweeps, and taper ratios and observe the results. The limiting factor for the resulting values was the crosswind performance, limited to 20% of the stall speed or 20 KIAS, whichever is largest, but not greater than 25 KIAS. Multiple trades were run, varying the size of the control surfaces and amount of sweep and taper, and relationships between these changes and the control speeds and frequencies were noted.

To begin with, the wing had a heavily restricted range of sweeps and taper ratios, only allowing up to around 30° of sweep with a taper ratio of around 0.8 or allowing a taper ratio of 0.2 with a sweep of around 20°. For adequate cruise performance and to meet the requirements of the customer, the cruise Mach number of the aircraft needed to be near transonic, limiting how low the sweep could be. As such, the sweep of the wing needed to be as large as possible while also keeping the taper ratio adequately low to allow for the aerodynamic design of the wing to be as simple as possible. This required the crosswind performance to be just above the required minimum. With the crosswind performance being the driving factor, designing for VMCA was difficult to do without making significant trade-offs on the crosswind performance. Fortunately, VMCA did not vary largely from changing the sweep and taper, only around 4-5 KIAS for acceptable designs, meaning designing for VMCA could be ignored without worry. VMCG, effectively, did not change at all with sweep and taper meaning it could be ignored in its entirety. Figure 34 displays the results of this trade.

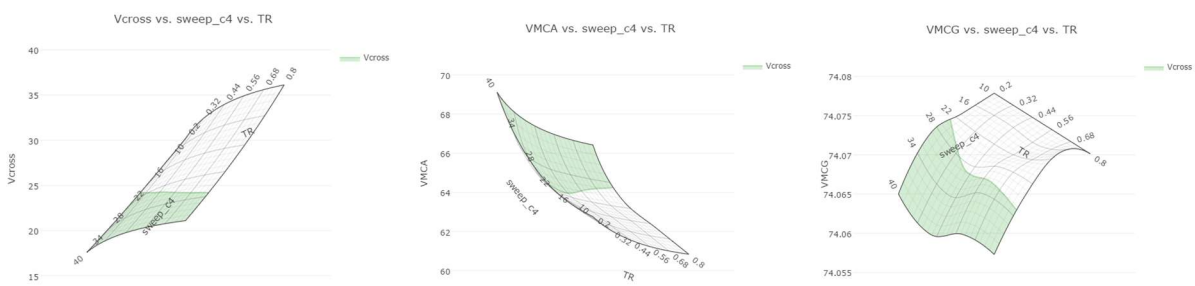

Figure 34. Control Speed Results Due to Sweep and Taper Ratio of Wing

Next, the aileron sizing needed to be determined, as the trades conducted on the wing sweep and taper ratio made apparent that the crosswind performance was heavily dependent on the aileron performance. This was due to the maximum sideslip angle being determined as the minimum of that allowed by the aileron and rudder, the former being significantly smaller than the latter. Through subsequent trades varying the aileron length and width (Figure 35, overleaf), it was determined that the aileron needed to be of relatively large size in order to meet crosswind requirements.

While the ailerons needed to be large, in order to keep weight low and to have enough space for the aft wing spar, we selected the smallest possible configuration that still complied with the requirements. This also had the added benefit of allowing for the most space for the flap system to be implemented, as the flaps would extend from side-of-body to the start of the ailerons. Because the crosswind performance, weight, and space management took precedence, the VMCA performance was ignored, though it was clear that it would be adequate so long as the crosswind requirement was met. Finally, aileron sizing had no effect on the VMCG performance whatsoever.

Rudder sizing was determined last. As previously explained, the crosswind performance was limited by the aileron size, meaning that the rudder was sized to optimize VMCA and VMCG as in Figure 36. It was found that increasing the height and width of the rudder decreased the values of the previously mentioned variable, as such a balance had to be found between weight and performance.

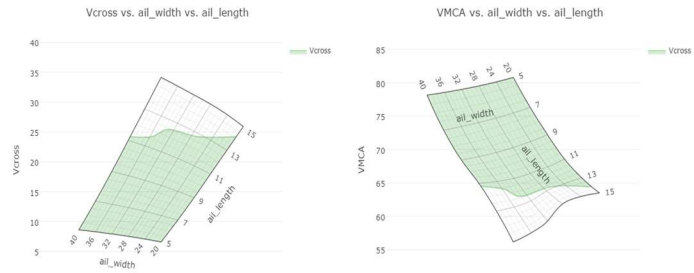

Figure 35. Control Speed Results Due to Aileron Size

Two wing position configurations were also considered throughout designing the aircraft. With the fuel tanks being mounted on the top of the fuselage, it made sense to consider a high wing configuration as the fuel system would need shorter insulated fuel lines, making accommodating the cryogenic fuel much simpler. Because of this, trades were run to see the difference in control speed performance for a standard low wing configuration and a less standard high wing configuration. Both cases varied the dihedral angle. The results in Figure 37 showed that the low wing configuration performed noticeably better than the high wing configuration at all dihedral angles for all control speeds. However, to be able to meet crosswind requirements, both wing configurations required a significant anhedral angle, which would pose a significant ground clearance problem for the low wing configuration engines.

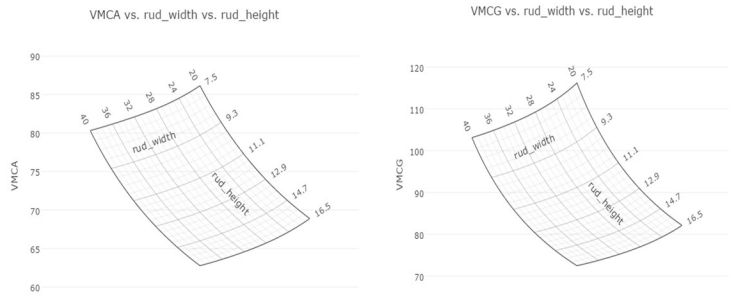

Figure 36. Control Speed Results Due to Rudder Size

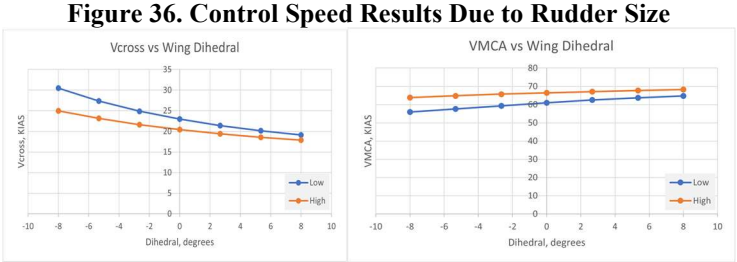

Figure 37. Crosswind Trim and VMCA Due to Wing Position and Dihedral Angle

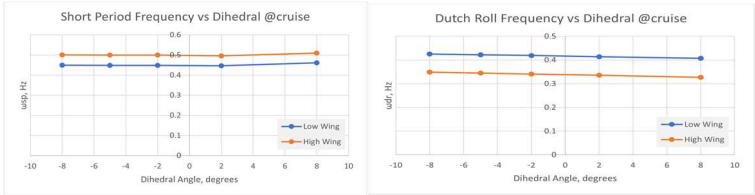

Figure 38. Short Period and Dutch Roll Frequencies for Various Dihedral Angles at Different Wing Positions

Throughout these trades, variations in the short period and Dutch Roll frequencies were largely ignored as it appeared that reaching adequate control speed performance also resulted in adequate performance in short period and Dutch Roll modes. However, wing placement was determined by the values of the frequencies. Through a simple trade which took a control wing design and varied the position of the wing and the dihedral angle, the optimal position for the wing was determined based on its respective trade-offs on the two frequencies.

Figure 38 shows that there is a larger trade-off for wing position with respect to the Dutch Roll frequency than for the short period frequency, meaning that it would be more beneficial to proceed with a high wing design in this instance. This, combined with the clearance issue stated previously, is what led to the selection of a high wing configuration for the aircraft.

J. Point Performance (Skymaps)

Using the Skymaps tool, trade studies were run for varying weights and engine scale factors to assess their impact on our aircraft's point performance, namely for its specific range.

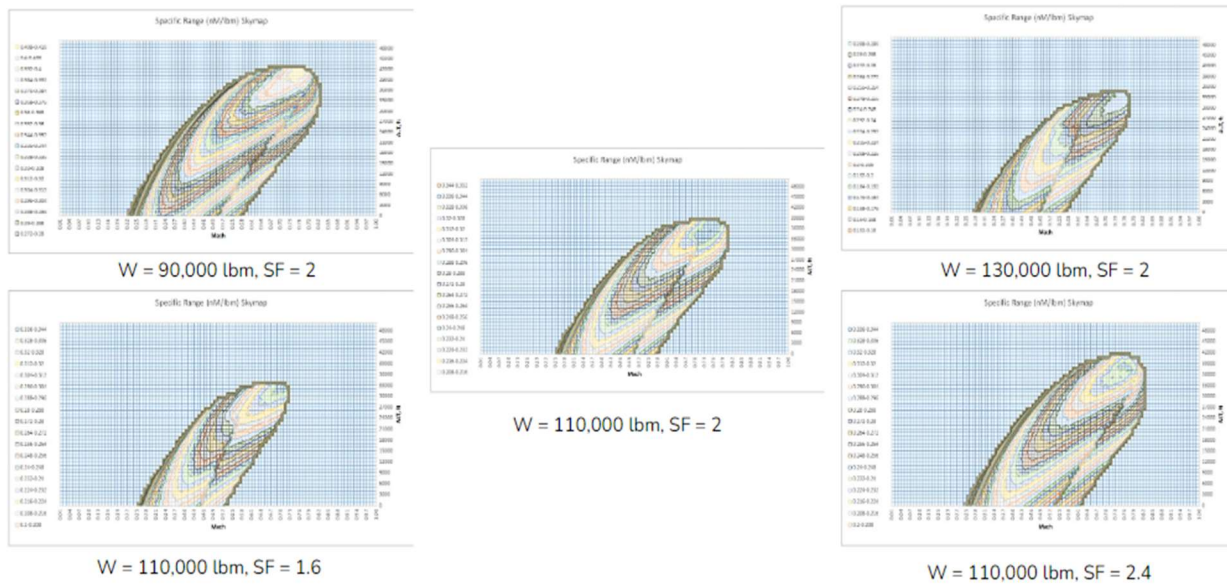

Figure 39. Specific Range for Changing Weight and Engine Scale Factor

In Figure 39 above, we examine the effect of varying aircraft weights and engine scale factors on the specific range performance of the aircraft. Ideally, a higher specific range is desired as this means that the aircraft can fly a larger distance for a given amount of fuel which indicates that our aircraft has very good fuel efficiency. From Figure 39, it was observed that increasing the weight of the aircraft reduces the specific range. For higher weights, flying at a higher Mach number and a lower altitude is required to achieve the best specific range for that given aircraft weight. It is also observed that as the engine scale factor is increased for a given weight, the best specific range is observed at a higher altitude and higher Mach number.

K. Field Performance

From our market study, we were able to determine what airports our customers operate out of, and therefore the runway length constraints of our aircraft. To determine how varying the lift coefficient affected the takeoff and landing performance, several trade studies were run. The results of these trade studies showed that as the lift coefficient increased, the runway length needed for both takeoff and landing decreased. The following plots display these trends.

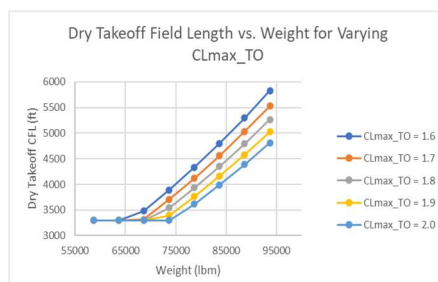

Figure 40. Dry Takeoff Field Length vs. Weight for Varying CL_{maxTO}

Note that for dry landing field length (Figure 41), the 115% factored length was most important since according to the CFR, the 115% factor of safety is used when there is a nearby airport with better runway capabilities. Also from this trade study, it was also discovered that for takeoff (Figure 40), it is not necessary for the lift coefficient to be as high as it would be for landing. The ideal takeoff lift coefficients were around 1.8-2.0 while the ideal landing lift coefficients were around 2.6-3.0.

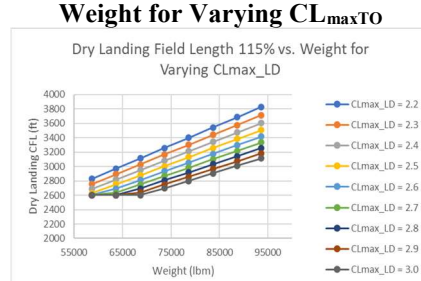

Figure 41. Dry Landing Field Length vs. Weight for Varying CL_{maxLD}

Another trade study in Figure 43 (overleaf) explored how engine scale factor affects the takeoff and landing performance. It was found

that increasing the engine scale factor decreased the required takeoff runway length. The following plot displays this trend. The engine scale factor had no effect on the landing performance of the aircraft.

The last trade study run explored the second segment one engine inoperative (OEI) climb gradient. Figures 43 and 44 show how the climb performance varies with takeoff lift coefficient and engine scale factor, respectively. The results show that the effect of the takeoff lift coefficient on climb is not very significant and as engine scale factor increases, the climb gradient increases.

L. Mission Performance (Mission Code)

The mission performance trade studies allowed us to fine tune certain attributes such as the engine scale factor and cruise conditions that are necessary to optimize performance.

Knowing that a two-engine design was the most optimal from the point of view of indirect operating cost, the scale factor had to be determined. Using four different trade studies at three different cruise distances helped determine the best scale factor for the two engines. We show only a few trade studies here which optimize the aircraft for a cruise distance of 600-nM. The scale factor range tested is a scale factor from 1.5-2.2 per engine. The cruise altitudes - when both plots are combined - range from 10,000-ft to 38,000-ft. NENG is the number of engines multiplied by the scale factor. The scale factor increases burns more fuel at lower altitudes. As shown in Figure 45b, a sweet spot can be seen for the best scale factor for the turbine engines. The sweet spot consists of a range between 1.5-1.9 and is visible in the 30,000-ft to 34,000-ft altitude range.

Further trade studies needed to be conducted to help determine the best scale factor over distances that would be conducted under popular missions for our plane. The next two plots in Figure 46 (overleaf) use the same scale factor range as the previous trade study, but utilizes a smaller and more realistic range of cruise altitudes from 20,000-ft to 38,000-ft. Figure 46a uses a cruise distance of 800-nM and 47b uses a cruise distance of 1200-nM. The plot for a cruise distance of 800-nM shows that the scale factor should be no greater than 2 since anything above performs worse than scale factors below. The plot for a cruise distance of 1200-nM shows that a scale factor between the range of 1.8 - 1.9 is the most optimal for total fuel burn across multiple cruise altitudes.

V. Design

A. Fuselage and Tanks

Some of the fuselage and tank design has been covered already from a conceptual level but there is still additional detail required for the final design. The insulation method is known in addition to how the tank lengths are set but the actual tank size and configuration & integration of support systems is not yet known. We decided that the

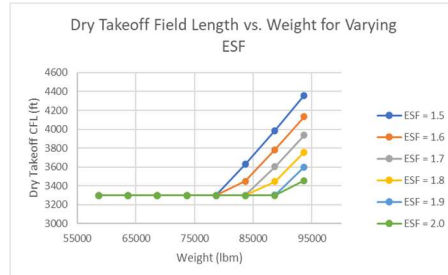

Figure 42. Dry Landing Field Length vs. Weight for Varying ESF

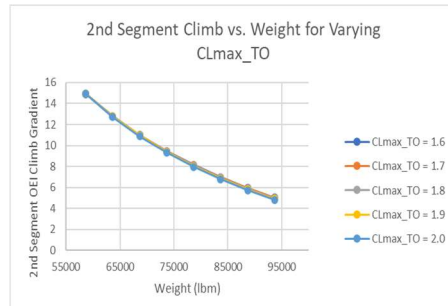

Figure 43. 2nd Segment OEI Climb for Varying CL_{maxTO}

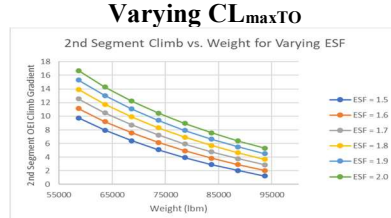

Figure 44. 2nd Segment OEI Climb for Varying ESF

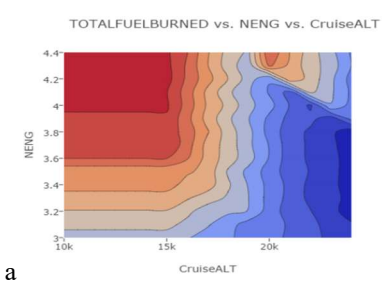

a

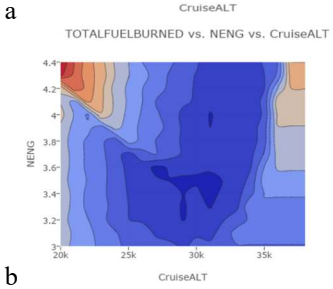

b

Figure 45. Scale Factor and Cruise Altitude Trade Study for 600-nM Cruise Distance

tank configuration shall include 3 radial tanks parted near the middle by the required rotor burst protection resulting in 6 total tanks. This configuration allows for greater structural efficiency while retaining a relatively regular cross section and being clear of rotor burst danger.

This fuselage must account for a set number of 88 passengers and 2 flight attendants. The interior design is in the following section but this relates to an external fuselage length of 93-ft and a cabin diameter of 132-in. This includes the largest diameter set by the seating arrangement including several-in for the fuselage wall structure. That sets the initial allowable tank length which will decrease due to the engine placement and rotor burst zone. This fuselage length accounts for the cockpit, extra tail length, and length for the vertical tail integration.

The individual tank diameter is set by the required maximum fuel of the aircraft. This comes from simulations considering sizing and mission performance which in turn sets a maximum fuel volume. The interactions are already known from the previous trade studies, it was just a matter of sizing the aircraft and tanks properly to meet all fuel requirements. With an external diameter of 54-in and a combined length (aft + fore tanks length) of 603-in the aircraft can carry the required fuel mass of 8,600-lbm relating to about 14,560-gallons of usable fuel. This is enough fuel for the longest expected journey at maximum payload with the proper fuel reserves. This accommodates the 88 passengers in the fuselage and all associated fuselage size requirements.

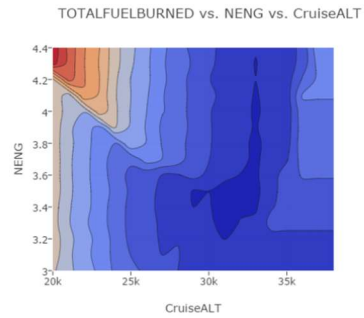

a

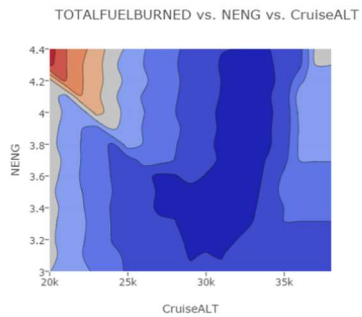

b

Figure 46. Scale Factor and Cruise Altitude Trade Study for 800-nM and 1200-nM Cruise Distance

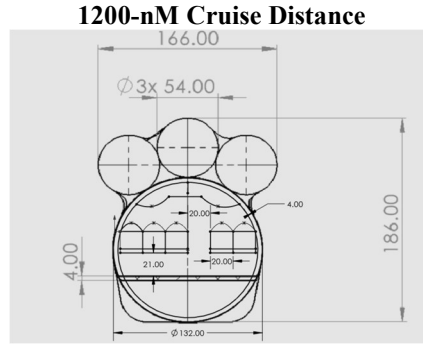

Figure 47. Fuselage Cross-Section

The cryogenic tank storage conditions are a variable parameter as well that can influence the design. As the storage temperature increases (not to exceed the critical point) the storage pressure must also increase with safe margins. This sets hard requirements on the tank structure as they must accommodate the required pressures. Our design settled on a storage temperature of -410 °F and a storage pressure of 140-lbf/in^2. The insulation gas (Xenon) pressure must be 20-lbf/in^2 as well in order to let the outer tank have internal pressure. This means an internal material thickness of 0.03-in using SS AM-350 and an external material thickness of 0.031-in using Aluminum 2024-T3. The tanks also include anti-sloshing plates that are 0.125 in thick also made from SS AM-350 with 7 plates in each of the 6 tanks. Each tank also includes insulating mounts made from a thermal insulator like ceramic. This reduced heat transfer to the comparatively hotter outer skin. This totals to a combined empty tank weight of 7270-lbm.

Refrigeration and insulations support systems are required to support the cryogenic fuel. This design did not attempt to go into depth completing the design of a rather uncommon fuel support system. Instead, we budgeted space and weight for these systems understanding that they must take up significant space and will likely be heavy.

All systems discussed here are accounted for in weight estimates. The weight of the refrigeration systems and insulation systems scales proportionally to the volume of maximum fuel. The team deemed it reasonable that 3000-lbm of refrigeration hardware would be sufficient to accommodate 12,000-gallons of fuel. A similar metric was used for the insulation system but at a lower weight. This accounts for all obvious requirements of the fuel system novel to this aircraft and the necessary integration concerns with a typical passenger cabin. View Figure 47 for a cross-section of the fuselage.

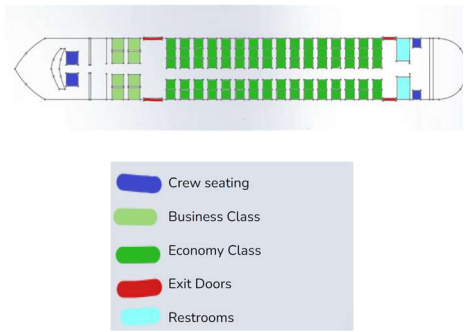

Figure 48. Interior Class Seating Set-Up

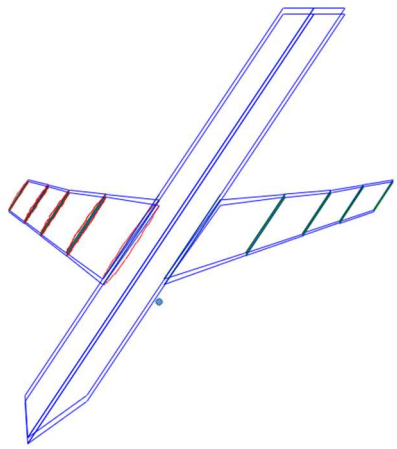

Figure 49. Camber/Sandwich Panel VORLAX model

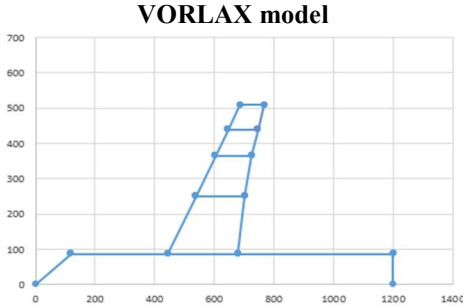

Figure 50. Wing Geometry and Control Points

B. Interior Layout

In reference to the interior design of the fuselage, Figure 48, the 14 CFR §121.311, §91.107, and §25.785 regulations were considered while also using the cabin sizing trade that considered the passenger count and their accompanying weight. This lead to the seating of up to 88 passengers and a minimum requirement of two pilots and two flight attendants totaling 92 people aboard the plane. As seen in the design, there are separate crew seating areas from the passengers in business class and economy class. For the business class seat pitch, the distance from each seat from back-to-back is 36-in and the economy class has a seat pitch of 31-in. The exit doors can be found at the front of the plane behind the business class and in the back of the plane behind the economy class. These exit doors are at 40.4-ft apart from each other, satisfying the 14 CFR §25.807 regulation to keep Type A doors within 110 passengers. The interior design also includes two restrooms and two workstations for the employees. These design elements require a total internal length of 74-ft. This leaves the rest of the length of the fuselage for more critical design aspects, such as fueling and controls and components.

C. Wing Design

A well-performing wing must meet its lift design criterion, its critical Mach number criterion, exhibit an elliptical lift distribution, and produce favorable isobar patterns. Using the design tools previously described (the WINGLETS tool) the geometry of the wing was chosen through an iterative design process. The wing design tool was first configured at the cruising conditions set by trade studies: Mach 0.76 at 33,000-ft altitude. The tool was then used to model a wing and fuselage combination in VORLAX, where the wing was simulated as a sandwich panel with variable camber, thickness, and twist, and the fuselage was simulated as two horizontal flat plates, as seen in Figure 49.

Five leading edge control points were then defined across the semispan, see Figure 50. At each control point, an airfoil was defined to produce a wing with a three-dimensional pressure field compliant with the critical Mach Number requirement. Recall that the critical Mach number is the lowest freestream Mach number at which the flow over some portion of the wing first goes sonic. To avoid shocks and satisfy the critical Mach number criterion, the pressure coefficient indicating a critical Mach number on the upper surface was calculated using Küchemann's equation for critical pressure coefficient (Cp*) seen in Eq. (8).

$$C_p * = \frac{2}{\gamma * M_\infty^2} * \left\{ \left(\frac{2}{\gamma+1}\right)^{\frac{\gamma}{\gamma-1}} * \left(\left(1 + \frac{\gamma-1}{2} * M_\infty^2 * cos^2\Lambda\right)^{\frac{\gamma}{\gamma-1}} - 1\right) \right\} \tag{8}$$

The resulting Cp* of several 2D sections across the span (wing/body junction, inner midspan, midspan, and outer midspan) were plotted alongside the upper and lower surface pressure distributions for each cross-section location. By keeping the pressure coefficients for the upper surface beneath the Cp* line, we can design against shocks. This was done by observing the upper surface pressure coefficients for each airfoil section as various camber and thickness forms were tested, which was shown earlier in the wing thickness trade studies.

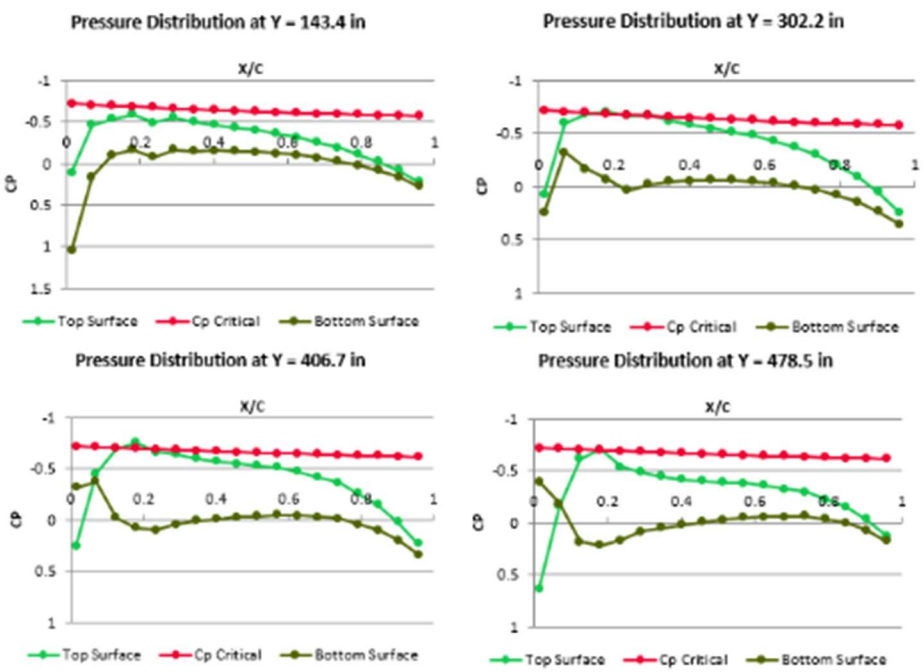

Figure 51. Pressure Distribution at Wing Spanwise Locations

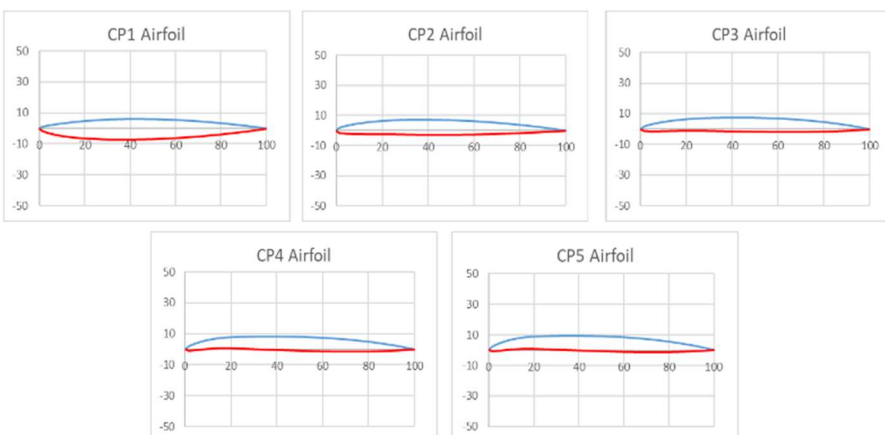

Location	Section Twist (degrees)
Side of body @ CP1	3
Inner Midspan @ CP2	0
Midspan @ CP3	-1
Outer Midspan @ CP4	-1.5
Tip @ CP5	-2

Figure 52. Wing Airfoil Geometry

Figure 51 shows the final pressure distributions for the specified cross sections of our wing. Since the upper surface pressure coefficients remain almost always greater than the critical pressure coefficients across the chord for each spanwise location, it is safe to say that shocks on the wing are minimal if present at all and thus the critical Mach number criterion is met. The airfoil geometries at each control point that resulted in these satisfactory pressure distributions can be seen in Figure 52.

These airfoils are combinations of different camber forms and thickness forms superimposed together with camber and thickness multipliers. Note that the camber is negative at the wing/body junction since Takahashi and Kurus note that it "helps improve pressure isobar alignment over the span of the wing" [14] and promotes suitable stall characteristics. In addition to satisfying the critical Mach number criterion, our wing design must also exhibit an elliptical lift distribution, which it does. Calculation of the ideal loading for this wing is in Eq. (9).

$$L'(y) = 1.226 * \sqrt{1 - \left[\frac{y}{b/2}\right]^2} * \frac{W}{S} * \underline{c} \tag{9}$$

By plotting the ideal lift distribution with the actual lift distribution for our wing, it was easy to see which sections of the wing needed adjustments to increase lift and minimize induced drag. Note that the lift generated by the fuselage was primarily characterized by the angle of attack inputted in VORLAX, although its magnitude was also dependent on the camber and incidence at the wing/body junction. To better match the ideal lift distribution for the fuselage section and to produce the desired lift, a 2° cruise angle of attack was selected. Making our wing's lift distribution elliptical was heavily dependent on the twist and camber for each control point. Camber and thickness were the main factors in satisfying the critical Mach number criterion but twist and camber played the largest role in creating elliptical loading. Increasing the camber of a control point increased the lift of the wing section and applying twist to a control point more drastically increased the wing section's lift along with surrounding wing sections.

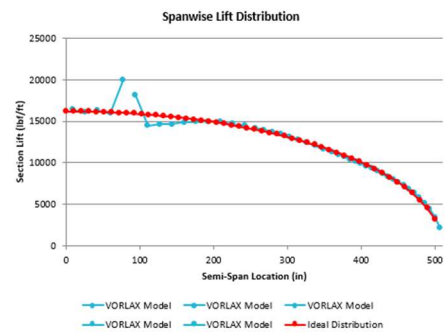

Figure 53. Spanwise Lift Distribution

As seen in Figure 53, our wing design produces an elliptical spanwise lift distribution for the most part. The spike present is a result of computational artifacts at the wing/body junction.

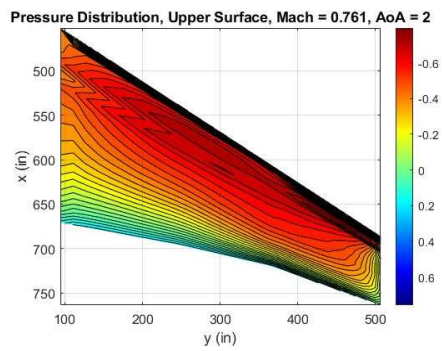

Figure 54. Wing Upper Surface Pressure Distribution (Isobar Contours)

To determine if the wing generated the required lift, the lift coefficient calculated in VORLAX was compared to the design lift coefficient at cruise calculated in Eq. (10) using the previously specified MTOW as the weight. Note that the VORLAX calculated lift coefficient is highly dependent upon the set angle of attack of the model, which again was set to 2° to ensure that the fuselage contributes enough lift to complete the "ellipse" while the overall wing achieves $C_{L_{design}}$

$$C_{L_{design}} = \frac{W}{q * S_{ref}} \tag{10}$$

The wing isobars were also plotted to ensure favorable isobar patterns were present (see Figure 54) for the final design geometry (see Figure 55): wingspan of 85-ft, a leading-edge sweep of 30.11°, a root chord length of 16.81-ft, a taper ratio of 0.4, a reference area of 1000-ft^2, and an anhedral angle of 8°.

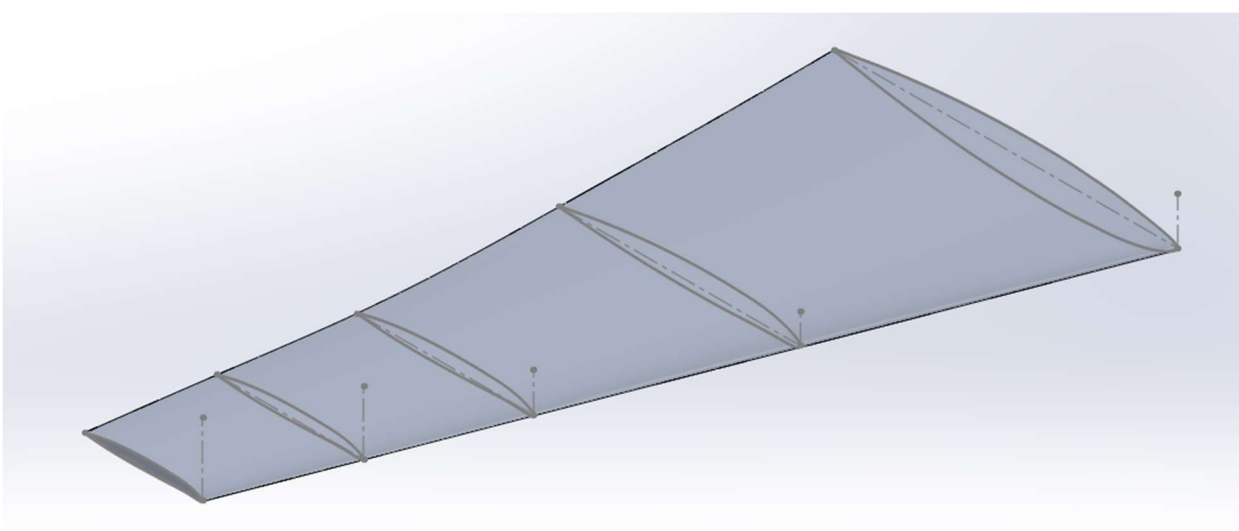

Figure 55. Wing Aerodynamic Design

D. Empennage

The empennage was designed in accordance with the results found from the trades conducted in previous sections. To keep the aircraft both spin and departure resistant, the vertical tail was sized to be quite large for an aircraft of its size class. The physical height of the vertical tail was chosen to be 16.5-ft long and the root chord was chosen to be 17-ft long. These dimensions were chosen so that the aircraft would be well within the spin and departure resistant region for a typical flight configuration, while also remaining within that region for any other weight configurations that may be flown. The taper ratio of the vertical tail was determined by the horizontal tail's root chord, as the tip chord of the vertical tail was decided to be the same length as the root chord of the horizontal tail, resulting in a taper ratio of about 0.59.

The horizontal tail was sized in a way to make it as small as possible while still providing adequate performance in terms of longitudinal stability and crosswind capability. Through the trades conducted, a span of 30-ft and root chord of 10-ft were chosen. These dimensions ensured that the aircraft remained longitudinally stable while still allowing necessary space for an effective elevator. The horizontal tail had a taper ratio of 0.3 which was chosen to improve crosswind performance while not while keeping the aircraft spin and departure resistant. Additionally, a 7° dihedral was chosen in order to give more effective height to the vertical tail without sacrificing weight or drag performance.

Both the horizontal tail and vertical tail had leading edge sweeps of around 34°, 34.75°, and 34.35°, respectively, to prevent the onset of shocks occurring on the tail before the wing. Both tails were also chosen to have a thickness of 10% chord, again to delay shock formation. Overall, the empennage (Figure 56) was adequately designed to perform up to the standards set by customer and CFR requirements.

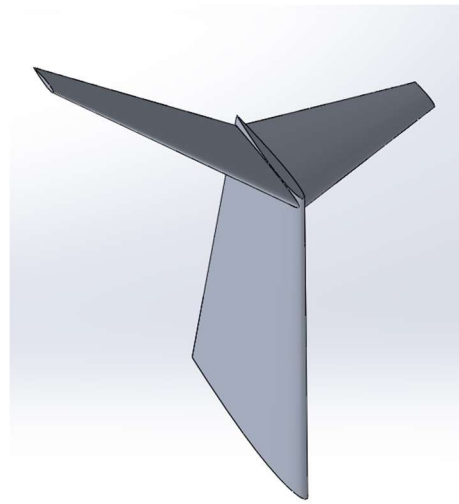

Figure 56. Final Empennage Configuration

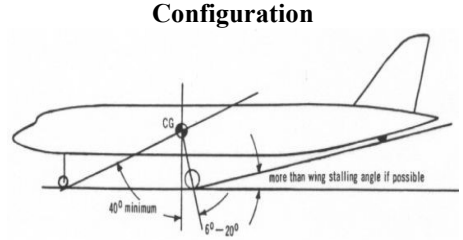

Figure 57. Landing Gear Position Limits [15]

Table 2. Landing Gear / Tire Sizing

	Main	Nose
Tire Size (in)	40 x 12	24 x 7.7
Inner Diameter (in)	18	10
Ply	20	16
Max Load (lbm)	24000	9725
Spar lengths (in)	78	78

E. Propulsion

The final propulsion system included two BPR=10 turbofans, modified for use with LH2, with 18,000-lbf sea-level static thrust per engine (an engine scale factor of 1.8).

F. Landing Gear

The nose and main landing gear was designed to retract into the fuselage as this is a high wing aircraft. The gear locations were selected in terms of the reference flight CG position – which lies 46-ft aft of the nose and 8-ft above the bottom of the fuselage.

Figure 57 shows the design approach and Table 2 shows the limits that were used to determine the exact locations of the landing gears [15]. The main gear should be between 6° and 20° from the center of gravity. For ideal performance, our aircraft will have the main gear located 20° from the center of gravity, resulting in it being 5.6-ft behind the center of gravity.

The tires used for our nose and main landing gears were chosen while considering the size and MTOW of our aircraft as well as a 1.07 factor of safety set by the CFR. TABLE 7 displays the dimensions of the tires. The aircraft will have twin-wheel bogeys for both nose and main gear. With four main gear tires and two nose gear tires, the maximum load our aircraft can handle lies around 115,450-lbm, which comfortably meets our 1.07 factored 93,633-lbm MTOW.

G. Final Weights & CG

Compared to the conventionally powered benchmark aircraft, the LH2 fueled SkyWhale is heavy; see Table 3. Consider its OEW predicted at 63,147-lb, as compared to the BAE 146, CRJ 900, and the E175 which are 51,342-lbm [17], 48,160-lbm [18] and 47,774-lbm [19], respectively.

The main components of the SkyWhale include the structure, propulsion, auxiliary systems, and cryogenic tank systems. The structural weight of the aircraft is mainly composed of the weights of the primary structure of the wing, horizontal & vertical tails, fins, fuselage without the cryogenic tanks, nosewheel, mainwheel, aerodynamic control surfaces and the crud weight. The structural weight for our aircraft's configuration is about 30,195-lbm. The propulsion weight of the aircraft is composed of the weight of the engines, the nacelles and pylons and the batteries (narrow body aircraft). The propulsion weight is about 6,758-lbm. The auxiliary systems weight of our aircraft is composed of the weights of the Auxiliary Power Unit (APU), instruments on board, hydraulics, basic electrical systems, avionics, furnishings and air conditioning. The general system's weight is about 12,222-lbm. The typical residual weight of the aircraft is composed of the weight of the unusable fuel, lubricants and the pilots. Each of these weights were found to be 944-lbm, 96-lbm and 350-lbm respectively. Finally, the cryogenic tank system weight is composed of the combined tank weight, tank insulation weight, tank refrigeration weight and the tank mount structure weight. The weight of the cryogenic system was found to be about 12,582-lbm.

Our design payload is set to be 22,000-lbm to accommodate all domestic and commuter flights. For an average mission length of about 475-nM, the implied maximum fuel weight is about 8,516-lbm while the standard reserve fuel weight is about 2,000-lbm. This standard reserve fuel weight accounts for any diversions that may need to happen in case of an emergency or unfavorable landing conditions.

CG travel due to the split fuel system is minimized due to the dry wings and split cryogenic systems; see Table 4. The mass moment of inertia values are strange for a normal transport aircraft; see Table 5. Most notably, the ratio between the yaw with respect to the roll moments of inertia, around 6, is significantly larger than a normal transport aircraft, around 2; see Table 6. This was something to take note of as it may affect other aspects of the flight control of the aircraft. For one, the "body heavy" mass properties will make the aircraft express its Dutch Roll mode as dominated by roll rather than yaw. Thus, a "yaw damper" applied to the rudder is likely to be ineffective.

Table 3. Final Design Weights

Sky Whale Weights	
MTOW	93-663-lbm
OEW	63,147-lbm
MZFW	85,147-lbm
MLW	89,141-lbm

Table 4. CG Build Up

	CG Location (ft)	
Weight Configuration	x	z
MTOW	45.64	2.43
Full PYLD, No front tanks	46.92	2.18
Full PYLD, No back tanks	44.81	2.22
Full PYLD, No fuel	46.10	1.95
No payload	46.09	4.08
No payload, no front tanks	47.82	3.87
No payload, no back tanks	45.01	3.91
No payload, no fuel	46.77	3.67
Percent Movement	3.23	13.78

Table 5. Mass-Moments-of-Inertia of the SkyWhale

Ixx	296000 slug-ft^2
Iyy	1632000 slug-ft^2
Izz	1750000 slug-ft^2

Table 6. Mass-Moments-of-Inertia of Representative Aircraft

Airplane	I_x (Slug-Ft^2)	I_y (Slug-Ft^2)	I_z (Slug-Ft^2)	I_y/I_x	Weight (Lb)
B-720	2.28×10^6	3.45×10^6	5.75×10^6	1.51	170,000
B-727	0.80×10^6	2.70×10^6	3.20×10^6	3.37	135,000
B-747	13.20×10^6	28.00×10^6	39.60×10^6	2.12	560,000
XB-70	1.45×10^6	16.50×10^6	18.00×10^6	11.40	300,000
SST	4.70×10^6	39.00×10^6	42.90×10^6	8.30	380,000
X-15	3,600	86,000	87,000	23.90	14,600

H. Exterior Design

When creating the exterior design of the aircraft, the optimum results of the trade studies were examined to ensure mission success. All sketches that follow have their dimensions in-in unless otherwise noted. The 3-view of the aircraft in Figure 58 displays the total length of the vertical tail and of the horizontal tail. The dihedral angle of the wing can also be noted with an angle of -8°. The design includes two engines attached to the high wing which are 30-ft apart from each other in reference to their centers.

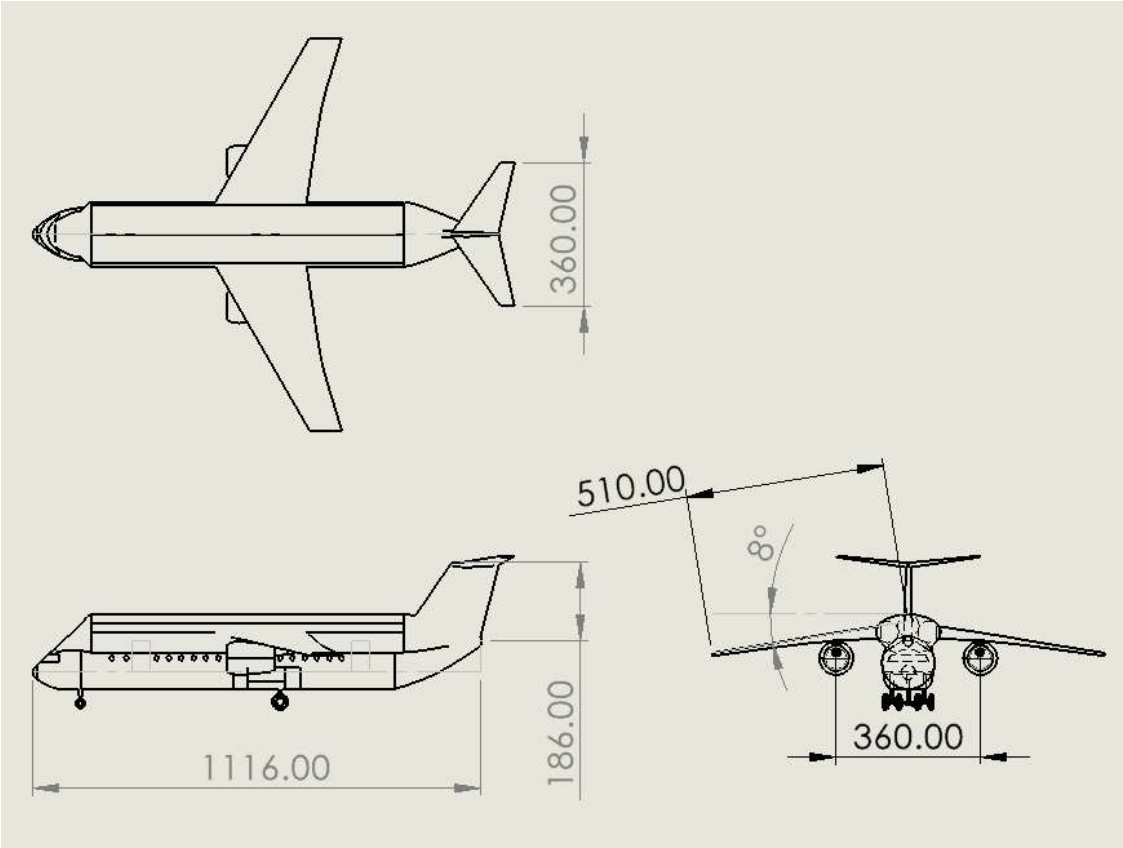

Figure 58. SkyWhale Three View

Figure 59. SkyWhale Rendering

VI. Technical Data Substantiating the Final Design

A. Stability and Control

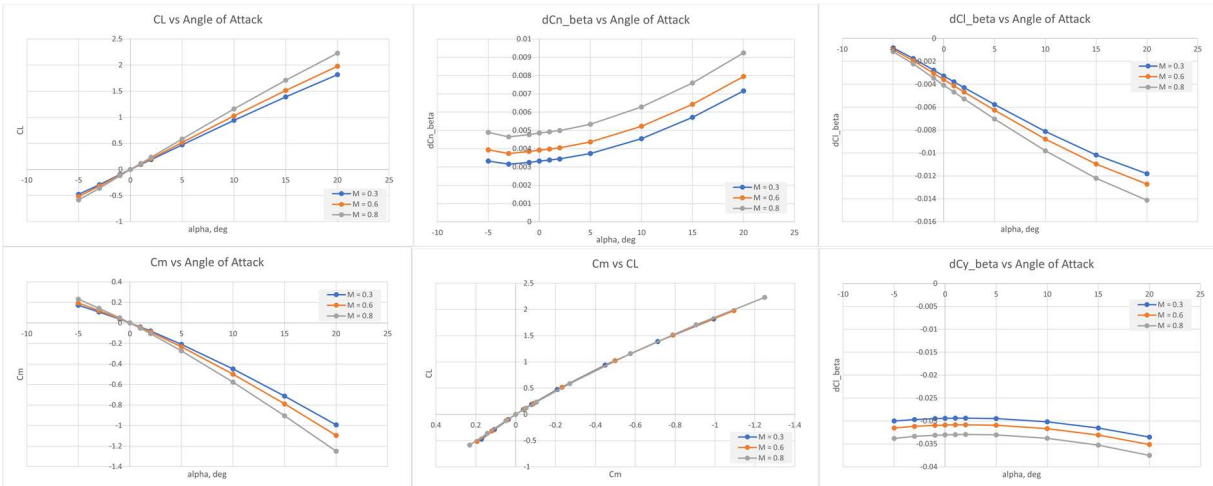

Figure 60. Basic Longitudinal and Lateral Stability Graphs

The aerodynamic database was developed using VORLAX. Here in Figure 60, we see that the SkyWhale is fully stable in pitch, roll, and yaw. For pitch, the slope of the pitch moment coefficient as a function of angle of attack is properly negative throughout the entire range of angles of attack tested. In addition, there is no negative pitch break as can be seen in the graph of pitch moment coefficient vs lift coefficient, as the trend is tending more negative, signifying a positive pitch break. In roll, the roll derivative with respect to the sideslip angle is negative for all angles of attack tested, while getting more negative as the angle of attack increases. Finally in yaw, the yaw derivative with respect to the sideslip angle is positive for all angles of attack, while getting more positive as the angle of attack increases. Also of note is that the side force derivative with respect to the sideslip angle is negative for the range of angles of attack, which is typical for most aircraft. Outside of the stability derivatives, it can also be seen that, even at an angle of attack of 20°, the aircraft still has not stalled, which will be necessary for the aircraft to achieve its desired maximum lift coefficient of 2.7 for landing.

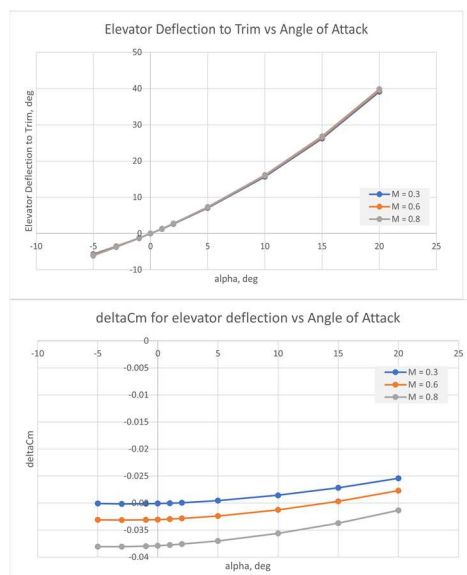

Figure 61. Defection for Trim and ΔCm for Deflection of Elevator as Functions of Angle of Attack

With the basic stability shown to be adequate, next was to determine the sizes of the various control surfaces. The elevator was designed first, as it behaved independently from the rudder and aileron since it played no part in determining control speeds required for takeoff. Determining the size of the elevator came down to ensuring the aircraft could properly trim at the necessary angles of attack for its various flight conditions. The final configuration's performance can be seen in Figure 61. We can see from this that the elevator has been properly sized, seeing as the required deflection for trim at all angles of attack is manageable for a given elevator. At cruise, the aircraft is designed to be flown at an angle of attack of 2°, meaning the associated elevator deflection required to trim is only around 2.5°, a very small deflection angle resulting in a small amount of drag increase.

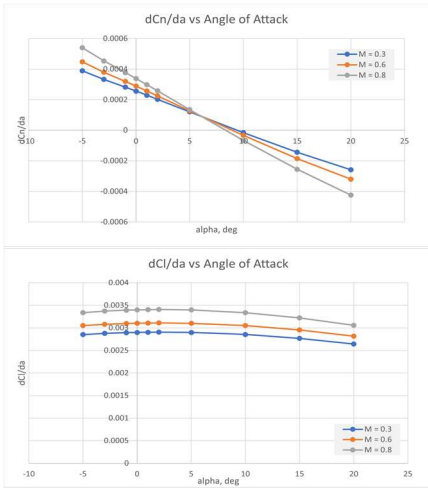

Figure 62. Aileron Performance in Yaw and Roll

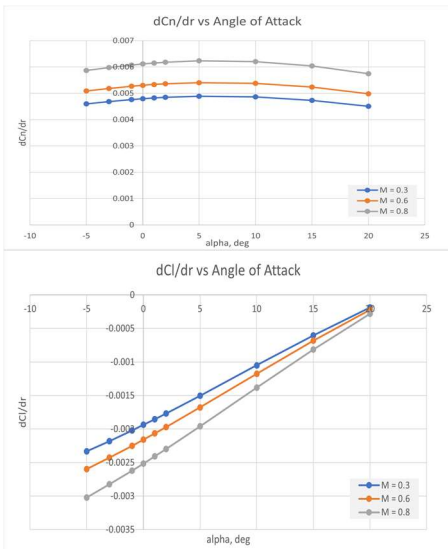

Figure 63. Rudder Performance in Yaw and Roll

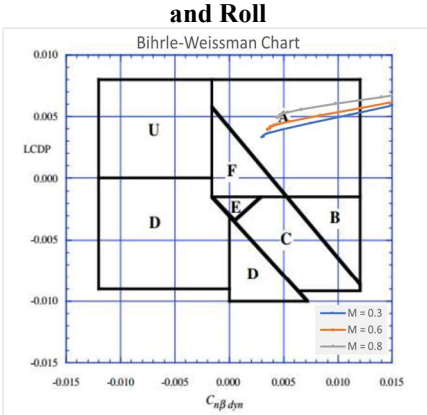

Figure 64. Bihrle-Weissman Chart for Final Configuration

Next, the aileron was sized, as the crosswind performance was limited by the size of the aileron. The aileron had to be sized relatively large in order for the aircraft to achieve the necessary crosswind requirements taking up 12-ft, around 28%, of the semispan and was also 35% of the chord width, resulting in an area of 34.2 square-ft for a single aileron.

Figure 62 shows how much the yaw moment and roll moment coefficients change per degree of aileron deflection for various angles of attack. Of note, the amount of yaw provided from the aileron is significantly lower than the amount of roll, around 10 times less or more at lower angles of attack. This large difference in response means that there is only a small coupling effect between the aileron yaw and roll modes, resulting in less rudder needed to counteract the yaw induced by a bank maneuver.

With the aileron sized, the rudder was free to be adjusted so that the VMCA and VMCG could be as small as possible while keeping the rudder small to reduce weight.

Figure 63 shows the amount of yaw coefficient and roll coefficient induced per degree of rudder deflection. Here, unlike with the aileron, there is a greater coupling between the yaw and roll mode due to the rudder. For low angles of attack, the increase in roll coefficient by deflecting the rudder is around a quarter of the increase in yaw coefficient, meaning that there is significant rolling induced when deflecting the rudder. This needs to be made note of as, combined with the unusual yaw-to-roll mass moments of inertia ratio from Table 4, there is going to be a rudder-aileron interconnect rather than the normal aileron-rudder interconnect found in most other transport aircraft.

The remaining performance data comes from post-processing the data found from the basic stability performance. The results displayed on Figure 64 show that the SkyWhale falls well within the A region of a Bihrle-Weissman chart, meaning that it is highly departure and spin resistant, which is exactly where it needs to be as a transport aircraft.

Next, the aircraft's longitudinal frequencies, short period and Dutch Roll, were calculated at four different points of a typical mission: takeoff, climb, cruise, and landing; see TABLE 7. These were compared to standards set in the MIL-SPEC 8785C handbook.

Table 7: Longitudinal Frequencies at Various Mission Conditions

Condition	ωsp (Hz)	ωsp (rad/s)	n/a	ωsp^2/(n/a)	ωdr (Hz)	ωdr (rad/s)
Takeoff	0.238	1.494	6.333	0.00892	0.393	2.471
Climb	0.340	2.134	12.925	0.00892	0.337	2.117
Cruise	0.372	2.338	15.265	0.00907	0.308	1.938
Approach	0.272	1.707	8.272	0.00892	0.350	2.202

For the short period frequency to fall within the level one region, the frequency must be greater than 0.14 Hz, which is the case for all mission conditions tested. Similarly, for the Dutch Roll frequencies to fall within the level one region, the frequency must be greater than 0.15 Hz, which is, again, the case for all mission conditions tested.

Next, the stall speeds for various flap settings needed to be known to ensure that the necessary crosswind capabilities are met, as well as to ensure stalling does not occur at takeoff and landing. To that end, three flap settings were used, for takeoff, cruise, and landing, and the following stall speeds were found in Table 8.

This assumed takeoff angle of attack was 10° with flap deflection at 20°, maximum angle of attack at cruise is 10° with flaps retracted, and landing angle of attack was 20° with flaps deflected 40°. These flap settings were necessary due to the lift performance required to meet runway requirements for our customers.

Finally, the various control and cue speeds for takeoff were found with the final aircraft configuration as seen in Tables 9.

Figure 65 shows the V-N diagram, or flight maneuvering envelope, for our aircraft. Per 14 CFR §25.337, the maximum positive load factor should be +2.5-gees; the minimum load factor is -1.0-gee.

B. Basic Aerodynamic Performance (Skymaps)

Table 10 shows the zero-lift-drag buildup of our final design developed by EDET. This model, along with the 5-column data from NPSS was used to generate point-performance "skymaps" as well as mission-performance flyouts.

Table 10. Zero-Lift-Drag Buildup from EDET

```
* CD0 BUILD-UP
* MACH NUMBER    ALTITUDE        REFERENCE AREA      TECHNOLOGY LEVEL
    0.78        35000. FT      1000.00 SQ FT          AITEK >= 1
*
* COMPONENT              SWET      LENGTH    FINENESS     FORM       RN        CF         CDF
                          SQ FT       FT       RATIO     FACTOR   MILLIONS
WING                    1837.00     11.76     0.1070      1.318     22.0    0.00247    0.00599
FUSELAGE                3274.58     93.00     6.2200      1.332    174.0    0.00183    0.00798
 V_Tail                  450.50     12.39     0.1000      1.297     23.2    0.00245    0.00143
 H_Tail                  393.90      4.88     0.1000      1.297      9.1    0.00285    0.00145
 Nacelle                 239.20      8.00     2.0000      2.641     15.0    0.00263    0.00166
 Pylon                   323.20      6.40     0.1000      1.297     12.0    0.00272    0.00114
ADDITIONAL-CD0                                                                          0.00000
ADDITIONAL-CD0                                                                          0.00000
ADDITIONAL-CD0                                                                          0.00000
ADDITIONAL-CD0                                                                          0.00000
CRUD/MISC/BASE                                                                          0.00586
TOTAL                   6518.38                                            0.00392     0.02552
```

As shown in Figure 66, the aerodynamic efficiency is highest within Mach 0.33 and 0.77 depending on the altitude being flown at, which is between 0-ft. and 36,000-ft. This plot was developed at MTOW, 93,663-lbm. With both Mach number and altitude changing, the maximum aerodynamic efficiency appears to occur when these two factors are changed relatively proportional to each other. For example, at lower Mach numbers, L/D is highest at lower altitudes. Likewise, L/D is maximized at higher altitudes when being flown

Table 8 – Stall Speed for Various Flap Settings

Condition	CL	Vs (KIAS)
Takeoff	1.9	121.097
Cruise	1.16	155.048
Landing	2.7	101.584

Table 9: Various Cue and Control Speeds

	Speed (KIAS)
V2	136.839
Vref	157.425
Vcross	25.038
VMCA	71.395
VMCG	82.888

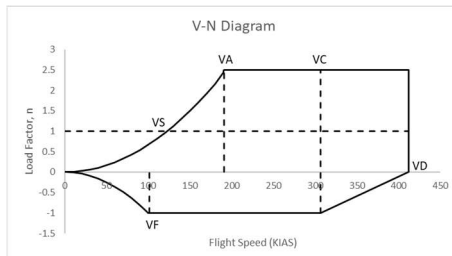

	Speed (KIAS)
VS	121.097
VA	191.62
VC	306.4
VD	412.33
VF	101.13

Figure 65. V-N Diagram

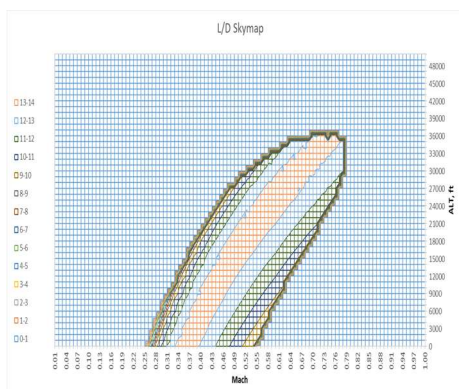

Figure 66. Aerodynamic Efficiency (L/D) @ MTOW

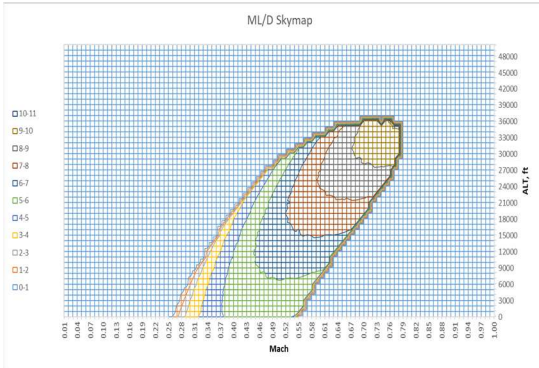

Figure 67. Aerodynamic Performance Efficiency (M(L/D)) @ MTOW

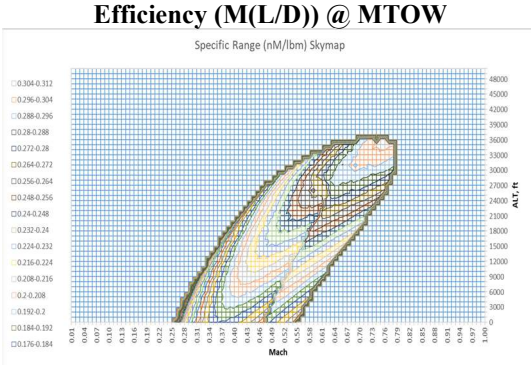

Figure 68. Specific Range @ MTOW

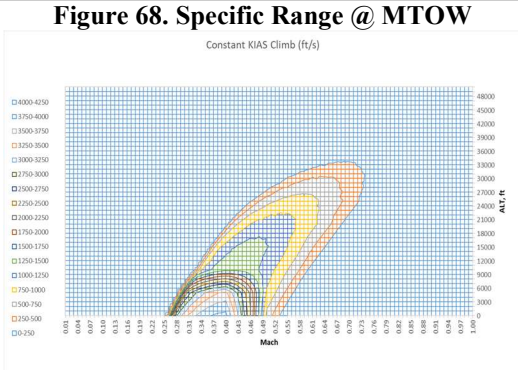

Figure 69. Rate of Climb @ MTOW

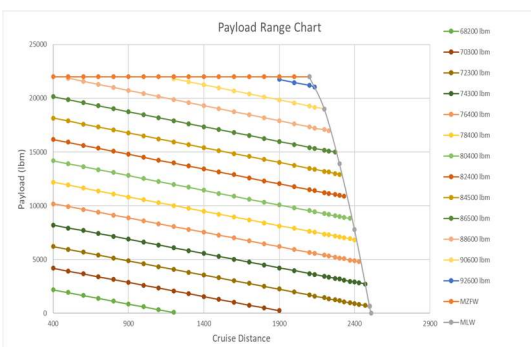

Figure 70. Payload/Range Chart (M=0.76 cruise)

at higher Mach numbers. This creates a "sweet spot" with respect to the combination of Mach number and altitude where L/D can be maximized at any Mach number or altitude.

The aerodynamic performance efficiency, whose behavior is shown in Figure 67, has a different trend compared to aerodynamic efficiency. M(L/D) is maximized at larger Mach numbers and higher altitudes, and it generally decreases as both Mach number and altitude decrease. This puts the optimal aerodynamic performance efficiency to occur between Mach 0.68 and 0.78 at altitudes of 28,000-ft to 36,000-ft.

As observed in Figure 68, the trend for specific range is somewhat similar to that of aerodynamic performance efficiency where it is highest at high Mach numbers and altitudes and generally decreases as Mach number and altitude are decreased.

Looking at Figure 69, it can be seen that within the allowable range of Mach numbers and altitudes, rate of climb is highest when either of these factors are at its extremes for any given value of the other factor (above Mach 0.53). For instance, at Mach 0.6, the rate of climb is maximum at 10,000-ft and 32,000-ft, which are the minimum and maximum allowable flight altitudes at that Mach number. Similarly, at 15,000-ft, the Mach numbers that would maximize the rate of climb are 0.36 and 0.64. These are the extremes of the Mach number allowed at that altitude. The same trend is seen for nearly all altitudes and for Mach numbers above 0.53, although it is interesting to note that the rate of climb becomes much more dependent on the altitude at lower altitudes below 10,000-ft as any small changes in altitude below this threshold result in a larger change in rate of climb.

C. Mission Performance

The mission performance of the plane is similar - if not better than - the competitor's, such as the CRJ 900, the BAE 146, and the E175. The longest range the plane can fly with the maximum payload is 2,100-nM. The plane's range is limited by the volumetric capacity of the fuel rather than the weight of the entire plane; see Figure 70.

The desirable cruise Mach for all missions will be a Mach number of 0.76.

D. Field Performance

Figures 71 and 72 show the takeoff and landing performance for our final aircraft design. The solid lines show the dry runway lengths, and the dotted lines show the wet runway lengths. The horizontal dashed line represents the minimum runway length our aircraft must operate at (from airports Key West and London City), and the vertical dashed line represents our aircraft's maximum landing weight. For takeoff, our aircraft exceeds the minimum runway requirements for both dry and wet conditions. For landing, our aircraft exceeds the runway requirements for dry landing conditions, including 115% factored. For 115% factored wet landing, it just meets the requirement but still allows for landing at our customer's shortest runways with our aircraft's maximum landing weight. Note that the line goes above the 5000-ft minimum runway length only for weights larger than the maximum landing weight, which are not applicable to realistic operation.

There does exist a takeoff limit when operating at London City Airport. Because of its location in the city, the minimum climb gradient is 7.2%. Figure 73 shows the second segment OEI climb performance for our aircraft's specified takeoff lift coefficient of 1.9 as well as the maximum landing weight limit. Based on this climb performance, the MTOW for London City is limited to roughly 84,000-lbm. This means that the passenger capacity will be limited to about 75% of its full capacity for domestic flights. While this is not ideal, London City is not a hub airport, and it was not feasible to cater the aircraft design to this constraint at the expense of other constraints.

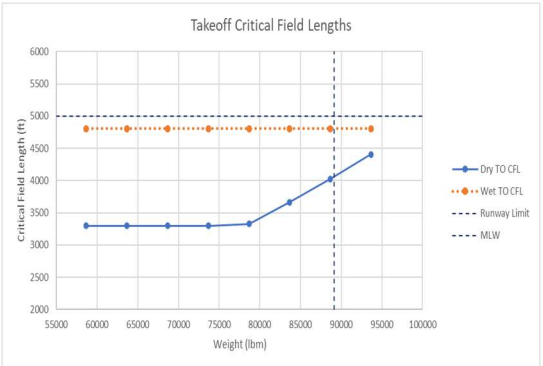

Figure 71. Takeoff Field Performance

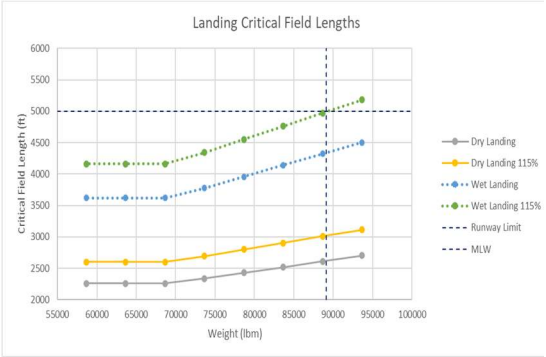

Figure 72. Landing Field Performance

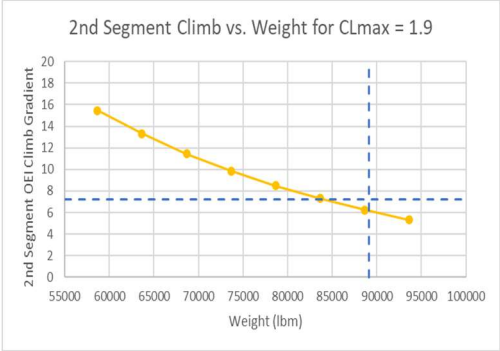

Figure 73. Second Segment OEI Climb Performance

VII. Conclusion

Our team was tasked with designing a regional jet that operates with zero carbon tail-pipe emissions. This jet is fueled by LH2 and aims to replace current operating regional jets fueled by kerosene. The zero emissions jet adheres to requirements outlined by both the customer and the Code of Federal Regulations. With these requirements in mind, our team utilized several design optimization tools and processes to achieve our goal. By using our developed design tools and conducting numerous trade studies to analyze SkyWhale's performance, we have concluded that our current detailed design can efficiently perform its designated flight missions. Our team has identified and satisfied all customer and system requirements and have successfully met all performance parameters. Our final design resulted in an 88-passenger, high wing with two underwing engines, T-tail configuration with top-mounted LH2 fuel tanks. The jet has an MTOW of 93,663-lbm with a maximum payload of 22,000-lbm, a maximum flight range of 2100-nM, and a cruise Mach number of 0.76.

Acknowledgments

This is a refined and evolved version of an undergraduate capstone project performed Spring semester 2022 at Arizona State University. Professor Takahashi wishes to thank Phoenix Integration for their generous support of *ModelCenter* for academic use. The team thanks Dr. Timothy Takahashi for his guidance throughout the aircraft design process. We also thank Joshua Heinz for his additional help as Professor Takahashi's graduate teaching assistant.

References

[1] "Facts & Figures," Air Transport Action Group, 2020, URL: https://www.atag.org/facts-FIGURES.html [retrieved 1 Feb 2022].
[2] Code of Federal Regulations, General, 2022.
[3] "Route Map", Delta Airlines, URL: https://www.delta.com/us/en/travel-planning-center/find-your-destination/route-map [retrieved 1 Feb 2022].
[4] "Route Map KLM", Flight Connections, URL: https://www.flightconnections.com/route-map-klm-kl [retrieved 1 Feb 2022].
[5] "Route Map Air France", Flight Connections, URL: https://www.flightconnections.com/route-map-air-france-af [retrieved 1 Feb 2022].
[6] Flight Calculator, Airplane Manager, URL: https://airplanemanager.com/flightcalculator.aspx retrieved [1 Feb 2022].
[7] AirNav, URL: airnav.com [retrieved 1 Feb 2022].
[8] Morrison, W. D., *Advanced Airfoil Design Empirically Based Transonic Aircraft-Drag Buildup Technique*, National Aeronautics and Space Administration, 1976.
[9] "Hydrogen," National Institute of Standards and Technology, 2021, URL: https://webbook.nist.gov/cgi/cbook.cgi?ID=C1333740&Mask=4 [retrieved 5 Feb 2022].
[10] *Metallic Materials and Elements for Aerospace Vehicle Structures*, MIL-HDBK-5J, U.S. Department of Defense, 2003.
[11] Miranda, L. R., Elliott, R. D., and Baker, W. M., *A Generalized Vortex Lattice Method for Subsonic and Supersonic Flow Applications*, National Aeronautics and Space Administration, 1977.
[12] Abbott, I. H., Von Doenhoff, A. E., Stivers, L. S., Jr., Langley Memorial Aeronautical Laboratory, Langley Field, VA, 1915.
[13] Takahashi, T., *Aircraft Performance and Sizing, Volume II: Applied Aerodynamic Design*, Momentum Press, New York, 2019.
[14] Kurus, N. J., Takahashi, T. T., and Perez, R. E., "Critical Mach number predictive methods for realistic supersonic wing / body configurations," AIAA AVIATION 2021 FORUM, 2021
[15] "Aircraft Landing Gear Layouts", Aerospaceweb.org, URL: http://www.aerospaceweb.org/question/design/q0200.shtml [retrieved 18 April 2022].
[16] Sartor, P. and Schmidt, R., Conceptual Design of a Hard Landing Indication System Using a Flight Parameter Sensor Simulation Model, *Research Gate,* URL: https://www.researchgate.net/FIGURE/Typical-Port-Main-Landing-Gear-Structure_fig1_266328768 [retrieved 12 April 2022].
[17] "British Aerospace BAe-146", Airliners, URL: https://www.airliners.net/aircraft-data/british-aerospace-bae-146/45 [retrieved 1 Feb 2022].
[18] "Bombardier CRJ 900 - Technical Specifications," GlobalAir.com, URL: https://www.globalair.com/aircraft-for-sale/Specifications?specid=1635 [retrieved 1 Feb 2022].
[19] "Embraer E175 - Technical Specifications." GlobalAir.com, URL: https://www.globalair.com/aircraft-for-sale/Specifications?specid=1364 [retrieved 1 Feb 2022].
[20] Takahashi, T., *Aircraft Performance and Sizing, Volume I: Fundamentals of Aircraft Performance*, Momentum Press, New York, 2019.
[21] Martinez-Rodriguez, G. and Takahashi, T.T., "Rapid Design of a High-Lift Wing Using Potential Flow Methods," Arizona State University, Tempe, AZ, 2022.